JOURNAL OF GEOPHYSICAL RESEARCH: OCEANS, VOL. 118, 227–243, doi:10.1029/2012JC008467, 2013

Remote sensing of salinity from satellite-derived CDOM in the Changjiang River dominated East China Sea

Yan Bai,[1] Delu Pan,[1] Wei-Jun Cai,[2] Xianqiang He,[1] Difeng Wang,[1] Bangyi Tao,[1] and Qiankun Zhu[1]

Received 20 August 2012; revised 5 November 2012; accepted 7 November 2012; published 29 January 2013.

[1] Defining highly variable freshwater plume area from space is important for characterizing the dynamics of biogeochemical properties and understanding the effects of climate change and human activities on plume-related processes. The absorption coefficient of colored dissolved organic matter (a_{CDOM}) from satellite ocean color data can be used to estimate the salinity and thus the plume area in coastal oceans if a robust conservative salinity and a_{CDOM} relationship and an accurate satellite a_{CDOM} algorithm can be established. In this paper, tight relationships between surface water salinity and *in situ* a_{CDOM} were found during several cruises covering all seasons and the full salinity range in the East China Sea. Thus, a salinity inversion model from a_{CDOM} was developed and validated with an independent data set, in which 73.6% of the data were within the absolute salinity error of ±1 and 87.1% were within ±1.5. Factors influencing the conservative behavior of colored dissolved organic matter are analyzed, with a particular focus on the effect of the phytoplankton-induced autochthonous colored dissolved organic matter. In addition, several satellite a_{CDOM} algorithms were compared and validated with our in situ data. Monthly satellite-derived salinity images were mapped in August from 2008 to 2010 and showed the significant interannual variability in the plume coverage. This study demonstrated that the salinity derived from satellite-derived a_{CDOM} can provide a reliable and good synoptic view of the plume area, and help with biogeochemical studies, in particular, those properties related to the interannual variability of plume coverage, although the development of a localized satellite algorithm of a_{CDOM} is still desirable.

Citation: Bai, Y., D. Pan, W.-J. Cai, X. He, D. Wang, B. Tao, and Q. Zhu (2013), Remote sensing of salinity from satellite-derived CDOM in the Changjiang River dominated East China Sea, *J. Geophys. Res. Oceans*, *118*, 227–243, doi:10.1029/2012JC008467.

1. Introduction

[2] Riverine freshwater plumes in ocean margins contrast greatly with surrounding waters with respect to their physical, chemical, and biological properties. Therefore, being able to define a plume area with a high space and time resolution is important for examining coastal ocean physical and biogeochemical processes, as well as for studying the impacts of human activities and climate change on coastal ocean processes. However, river plumes are highly dynamic in both space and time, and they are often difficult to define from limited field surveys. Thus, it is of great interest to characterize river plumes from satellite observations.

[3] Salinity is a direct indicator of a freshwater plume. Two specific microwave satellite sensors (*L*-band radiometers), the SMOS (the Soil Moisture and Ocean Salinity) and Aquarius/SAC-D satellite, were launched recently to directly monitor the global ocean surface water salinity. However, due to land contamination, coarse spatial resolution (typically 30–300 km), and long revisiting time (3 days or more) [*Koblinsky et al*., 2003; *Lagerloef et al*., 2008; *Font et al*., 2010; *Kerr et al*., 2010], the capacity to observe salinity in the coastal area and produce satisfactory salinity fields remains limited.

[4] Like sea salt, colored (or chromophoric) dissolved organic matter (CDOM), which is characterized by its optical absorption coefficient, a_{CDOM}, is also a soluble matter with distinct values in river and marine end-members [*Blough and Del Vecchio*, 2002]. In many large river estuaries and plume systems where physical mixing prevails, a_{CDOM} behaves conservatively and has good negative correlations with salinity [e.g., *Siddorn et al*., 2001; *Johnson et al*., 2003; *Chen and Gardner*, 2004; *Chen et al*., 2004; *Hong et al*., 2005; *Guo et al*., 2007; *Bowers and Brett*, 2008; *Stedmon and Markager*, 2001; *Stedmon et al*., 2010]. Therefore, in recent years, a_{CDOM} derived from satellite ocean color data has been used to estimate salinities in river-plume dominated coastal oceans, such as the areas receiving the Columbia River

[1]State Key Laboratory of Satellite Ocean Environment Dynamics, Second Institute of Oceanography of State Oceanic Administration, Hangzhou, China.
[2]School of Marine Science and Policy, University of Delaware, Newark, Delaware, USA.

Corresponding author: Y. Bai, State Key Laboratory of Satellite Ocean Environment Dynamics, Second Institute of Oceanography of State Oceanic Administration, 36 Baochubei Road, Hangzhou 310012, China. (baiyan_ocean@126.com)

2169-9275/13/2012JC008467

[*Palacios et al*., 2009], the Amazon and Orinoco rivers [*Hu et al*., 2004; *Del Vecchio and Subramaniam*, 2004; *Molleri et al*., 2010], the Mississippi River [*Del Castillo and Miller*, 2008], and the Clyde Sea [*Binding and Bowers*, 2003]. However, the relationships between salinity and a_{CDOM} have distinct local features in coastal oceans with different freshwater and marine end-members, and are regulated by regional hydrodynamic and biogeochemical processes. Therefore, it is generally not practical to apply a locally developed salinity-a_{CDOM} relationship to other areas, and sufficient field measurements are usually needed to parameterize the algorithm locally.

[5] The Changjiang (a.k.a. Yangtze) River is the largest river on the Eurasian continent and one of the largest rivers in the world. It discharges into the East China Sea (ECS), which is one of the widest continental shelves and one of the most productive marginal seas in the world. The Changjiang River plume (a.k.a. Changjiang Diluted Water (CDW), a name popularly used in the regional scientific literature) can travel northeastward over 450 km offshore to the Cheju Island in summer [*Moon et al*., 2009], and even affect the Sea of Japan [*Fang et al*., 1991]. It is of significance to study the Changjiang River plume-influenced ECS to understand marginal sea biological processes, and carbon and nutrient transport and transformation [*Tsunogai et al*., 1999; *Isobe and Matsuno*, 2008; *Chen et al*., 2008; *Gong et al*., 2011]. Yet, relative to other large river plume systems, few studies have been conducted on the optical characteristics of CDOM and their relationships with salinity in the Changjiang River plume, because in situ optical data are very limited [*Gong*, 2004; *Guo et al*., 2007]. *Sasaki et al*. [2008] and *Ahn et al*. [2008] attempted to use satellite data to map the Changjiang River plume. However, they used limited field data covering only the outer shelf with salinity greater than 29. As such, their algorithms must be evaluated in the river's lower-salinity plume area.

[6] In addition to the development of regionally specific salinity-a_{CDOM} relationships, the development of an appropriate satellite algorithm for a_{CDOM} is also a key challenge for mapping coastal oceans salinity using satellite ocean color data. Together with dissolved riverine matter, high concentrations of terrestrial detritus are also a feature of coastal oceans. In terms of a satellite algorithm, it remains difficult to separate the absorption coefficient of CDOM and nonpigmented organic particles (NAP) because they have similar absorption spectra with exponential wavelengths decay functions. As a compromise, a method using the combined absorption coefficient of CDOM and NAP, known as CDM and characterized by $a_{CDM}[\equiv a_{CDOM}+a_{NAP}]$, has been adopted for a_{CDOM} usage as long as the a_{CDOM} is overwhelmingly greater than the a_{NAP} [*Siegel et al*., 2002; *Sasaki et al*., 2008; *Molleri et al*., 2010]. This approach has worked in open ocean and clean shelf waters, but has generally failed in particle-rich waters, a scenario expected in the nearshore ECS. Based on the quasi-analytical algorithms (QAA) [*Lee et al*., 2002, *Lee*, 2006], *Zhu et al*. [2011] recently developed an extended QAA (QAA-E) algorithm to retrieve a_{CDOM} from QAA-derived a_{CDM} ($a_{CDOM}=a_{CDM}-a_{NAP}$). The QAA-E is expected to have wider applicability due to its analytical basis. However, more validations are required to further improve the QAA-E algorithm [*Zhu et al*., 2011], especially outside the Mississippi and Atchafalaya River plume region where the algorithm was developed.

[7] In the past 5 years, we have carried out nine cruises to measure water optical properties in the ECS, covering all seasons and the complete salinity range, from freshwater to high-salinity marine end-members (the Kuroshio water in the eastern boundary of the ECS). This abundant data set has allowed us to develop a more robust satellite algorithm for salinity and plume area detection. In this paper, first, field data are presented and the relationships between salinity and a_{CDOM} and their seasonality are analyzed. Then, several existing a_{CDOM} inversion algorithms are evaluated, and corresponding satellite-derived salinity maps are generated to show the applicability of these inversion algorithms, particularly in illustrating the interannual variation of the plume. In the discussion sections, the factors influencing the conservative behavior of CDOM are analyzed, with a particular focus on the effect of the phytoplankton-induced autochthonous CDOM. Finally, deviations between the observations and satellite-derived salinity maps are discussed with respect to future improvements.

2. Data and Method

[8] Nine cruises were conducted in the ECS from 2006 to 2011 (Figure 1 and Table 1): (1) Four cruises were carried out during the "908 Project" (hereinafter, C908) using the marine surveillance ships of the State Oceanic Administration, with the summer cruise covering a period from 19 July to 22 August 2006, the winter cruise from 24 December 2006 to 3 February 2007, the spring cruise from 4 April to 8 May 2007, and the autumn cruise from 13 October to 1 November 2007. (2) Another four cruises were carried out during the "973 CHOICE-C Project" (hereinafter, C973) in the ECS using R/V *Dongfanghong II*, with the summer cruise covering a period during 16–31 August 2009, the winter cruise from 24 December 2009 to 3 January 2010, the autumn cruise from 29 November to 9 December 2010, and the spring cruise from 31 May to 8 June 2011. (3) Finally, one additional cruise was carried out in the Changjiang Estuary and Hangzhou Bay during 23–28 September 2009 (hereinafter, CCJE-Sept) by the fishing boat *Zhouchongyu No. #24522*. The shipboard measured data used in this paper included surface water salinity, a_{CDOM}, chlorophyll *a* concentration, and remote sensing reflectance just above the sea surface.

[9] On the "C908" and "C973" cruises, the salinity profiles at each station were measured with a SeaBird CTD (SBE 917 and SBE 911plus, respectively). On the CCJE-Sept cruise, the surface water salinity was measured with a multiparameter water quality instrument, the RBR (XR-620). The underway surface water salinity was also measured on the C973 summer cruise at a measuring frequency of 1 min using an Idronaut Multiparameter "Flow Through" CTD, which was corrected by the salinity measured with the shipboard SeaBird CTD.

[10] The CDOM sample collection, storage, and measurement were performed according to Ocean Optics Protocols Version 2.0 [*Mitchell et al*., 2000]. Water samples were filtered through a Millipore™ glass filtration system with 0.2 μm polycarbonate filters at a low vacuum less than around 125 mmHg. The polycarbonate filters were presoaked in 10% hydrochloric acid (HCl) for about 15 min and rinsed thoroughly before filtration. The filtration system was cleaned in sequence with about 200 mL of Milli-Q purified water and a 200 mL seawater sample. The water sample was then

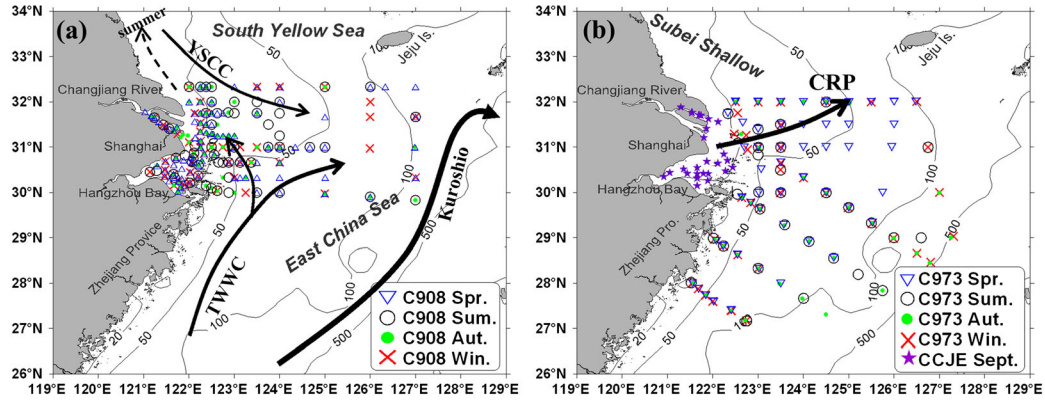

Figure 1. Research area and sampling stations. (a) Four C908 cruises (2006–2007) in the north ECS. (b) Four C973 cruises (2009–2011) and one cruise in the Changjiang Estuary and Hangzhou Bay (September 2009). Contours are in meters. The arrows indicate the Yellow Sea Coastal Current (YSCC), the Taiwan Warm Current (TWWC), the Kuroshio Current, and the Changjiang River Plume (CRP).

Table 1. Regression Results of Salinity and the Absorption Coefficient of Colored Dissolved Organic Matter (a_{CDOM}) at 355, 400, and 412 nm[a]

	Salinity Range(psu)			$a_{CDOM}(355)$				$a_{CDOM}(400)$				$a_{CDOM}(412)$			
Cruise	Min	Max	*N*	*A*	*B*	*R*	SD	*A*	*B*	*R*	SD	*A*	*B*	*R*	SD
C908-Spr.1[b]	0.62	34.52	91	37.216	–17.163	–0.94	3.33	37.918	–34.771	–0.91	3.96	38.108	–41.198	–0.90	4.20
C908-Spr.2[b]	7.03	32.98	68	35.224	–13.840	–0.88	2.98	35.358	–26.664	–0.85	3.28	35.357	–31.022	–0.84	3.39
C908-Sum.1	1.03	33.73	57	35.743	–14.841	–0.96	2.45	35.503	–29.975	–0.95	2.78	35.453	–35.712	–0.94	2.94
C908-Sum.2	10.02	32.76	48	35.032	–13.699	–0.93	2.46	34.802	–27.767	–0.91	2.76	34.743	–33.094	–0.90	2.90
C908-Aut.1	0.07	34.30	65	38.980	–17.609	–0.95	3.51	39.315	–37.645	–0.92	4.31	39.402	–45.299	–0.91	4.63
C908-Aut.2	4.10	32.95	45	38.280	–16.007	–0.92	3.26	37.989	-32.994	–0.88	3.93	37.828	–39.151	–0.86	4.20
C908-Win.1	0.38	34.31	51	37.189	–17.737	–0.94	3.28	37.649	–37.369	–0.92	3.83	37.788	–44.914	–0.91	4.03
C908-Win.2	15.16	32.88	31	34.545	–13.659	–0.78	3.72	33.980	–26.073	–0.73	4.11	33.735	–30.182	–0.71	4.24
C908all.1[c]	0.07	34.52	264	37.201	–16.713	–0.94	3.28	37.557	–34.637	-0.92	3.87	37.643	–41.328	–0.91	4.11
C908all.2	4.10	32.98	192	35.595	–14.151	–0.89	3.10	35.599	–28.545	–0.86	3.49	35.533	–33.639	–0.84	3.66
CCJE-Sept.	0.22	25.19	26	33.105	–13.292	–0.88	2.65	33.054	–29.613	–0.85	2.94	32.843	–35.811	–0.84	3.06
C973-Spr.	28.27	34.35	57	34.191	–7.370	–0.74	0.87	33.942	–13.525	–0.70	0.92	33.917	–15.867	–0.70	0.93
C973-Sum.	24.73	34.59	28	35.157	–12.626	–0.86	1.48	34.516	–21.446	-0.71	2.07	34.263	–23.046	–0.66[d]	2.21
C973-Aut.	27.38	34.60	35	35.559	–12.991	–0.96	0.59	35.856	–28.172	–0.94	0.69	35.959	–34.202	–0.93	0.74
C973-Win.	27.06	34.62	43	35.353	–11.923	–0.94	0.69	35.510	–25.843	–0.90	0.86	35.536	–30.978	–0.89	0.92
C973all[c]	24.73	34.62	163	35.217	–11.397	–0.88	0.99	35.095	–22.103	–0.81	1.22	35.041	–25.520	–0.79	1.28

[a]The linear regression equation is $Y=A+B\times X$, where Y is the salinity, and X is the a_{CDOM} at 355, 400, or 412 nm. A and B are the offset and slope, respectively; R and SD are the regression coefficient and standard deviation, respectively. Salinity Range shows the min and max values; and N is the number of valid samples.

[b]Postfix number "1" with the C908 cruise name indicated that the regression includes all of the measured data, while number "2" indicated that the regression used only the data with salinity ranging from 2 to 33.

[c]"C908all" or "C973all" indicated that the regressions use the pooled C908 data (or C973 data) from the four seasons.

[d]All the regression results are with the $p<0.0001$, except for the C973-sum with $a_{CDOM}(412)$, where $p=0.000145$.

filtered and placed directly into 60 mL CNW^{TM} brown glass bottles with Teflon gaskets. Before the cruises, the glass bottles were soaked in 10% HCl, rinsed with Milli-Q purified water, dried, and combusted at 450 °C for 4 h. The glass bottles with the CDOM samples were stored in refrigerators at –20 °C and were measured in the laboratory within 1 month after the cruise. In the laboratory, the optical densities (ODs) of CDOM samples were measured in a 10 cm quartz cell using a Perkin Elmer^{TM} lambda 35 ultraviolet-visible light spectrophotometer. The Milli-Q water was used as the blank with a flat baseline between ±0.0005 OD. The a_{CDOM} was calculated with:

$$a_{CDOM}(\lambda) = (2.303/l) \times \left\{\left[OD_{CDOM}(\lambda) - OD_{Milli\text{-}Q}(\lambda)\right] - OD_{null}(\lambda_0)\right\}, \quad (1)$$

where λ indicates the wavelength of the optic measurement and l is the quartz cell path length (0.1 m). $OD_{null}(\lambda_0)$ is the residual offset at the long wavelength (λ_0), and we used the average values between 695 and 705 nm as the residual correction (baseline correction).

[11] The water samples for chlorophyll *a* (*chla*) were filtered onto 25 mm Whatman GF/F filters with 0.7 μm pore size at a low vacuum. The filters were preserved in liquid nitrogen before being processed. Each filter was analyzed fluorometrically with a Turner-Design10 fluorometer to obtain the *chla* concentration. In this study, we used only surface layer samples for CDOM and *chla* (less than 5 m depth).

[12] The above-surface remote sensing reflectance, $R_{rs}(\lambda)$, was measured aboard ship using the above-water method [*Mueller et al.*, 2003]. An ASD (Analytical Spectral

Devices) FieldSpec HandHeld Spectroradiometer (FSHH, 325–1075 nm) was used to measure the upward radiances from the sea-surface (L_t) and standard reflecting plate (L_p) and the downward sky radiance (L_{sky}). To avoid Sun-glint contamination, the zenith and azimuth angles for measuring L_t were about 40° and 135° (referring to solar orientation), respectively. In addition, we selected the optimal place to minimize the effects of ship shading and foam. We set the integrating time according to the incident radiance intensity, and corrected the dark current for each change of integrating time. The ASD spectrometer was calibrated before and after each cruise using an NIST (National Institute of Standards and Technology) traceable irradiance lamp standard (OLFEL-1000) and a Spectralon plaque standard (Labsphere Inc.). According to the radiances measured by ASD FSHH, remote sensing reflectance (R_{rs}) can be calculated as

$$R_{rs}(\lambda) = \beta_p(\lambda)\left[L_t(\lambda) - \beta_s(\lambda_0)L_{sky}(\lambda)\right] / \left[\pi L_p(\lambda)\right], \quad (2)$$

where β_p and β_s are the reflectances of the standard plate and air-sea interface, respectively. In general, β_s varies from 0.022 to 0.05 [*Lee et al.*, 1996]. Here we estimated $\beta_s(\lambda_0)$ by assuming a black ocean at a near-infrared wavelength (λ_0) and wavelength independence [*Doxaran et al.*, 2002]. The λ_0 we used changed with the water turbidity, indicating longer wavelengths for more turbid. In addition, for the extremely turbid waters with high values in the near-infrared wavelength, we fixed β_s as 0.05 when the estimated value was larger than 0.05.

[13] In addition to our field measurements, we also used two global data sets to validate of the a_{CDOM} algorithm. The first was the International Ocean-Colour Coordinating Group (IOCCG) synthetic data set at 30° solar zenith angle, taken from the IOCCG website (http://www.ioccg.gov). It contains 500 records, with the shortest wavelength at 400 nm for both a_{CDOM} and R_{rs}. The data set was simulated by Hydrolight® and covered a wide range of natural water variations. The second data set was the global in situ NASA bio-Optical Marine Algorithm Data Set (NOMAD) data set (version 1.3), taken from the SeaBASS website (http://seabass.gsfc.nasa.gov) [*Werdell and Bailey*, 2005]. It contains 192 effective records, with the shortest wavelength at 405 nm for both a_{CDOM} and R_{rs}.

[14] The satellite data were downloaded from the NASA ocean color website (http: //oceancolor.gsfc.nasa.gov/). In this study, daily Moderate Resolution Imaging Spectroradiometer (MODIS)/Aqua products of R_{rs} at the 412, 443, 488, 531, 547, and 667 nm sensor bands with a spatial resolution of about 4 km were used.

3. Algorithms and Results

3.1. Relationships Between Salinity and a_{CDOM}

[15] The absorption spectrum of CDOM is a decaying exponential function of the wavelength as $a_{CDOM}(\lambda) = a_{CDOM}(\lambda_0) \times e^{S_{CDOM}(\lambda_0-\lambda)}$, where λ_0 is the reference wavelength and S_{CDOM} is the spectral slope. Here we used linear regressions between sea surface salinity and a_{CDOM} at three different wavelengths (355, 400, and 412 nm) because 355 and 400 nm are the commonly used wavelengths in CDOM biogeochemical research, and 412 nm is the shortest wavelength of the current ocean color satellite sensors. In the following sections, we describe the salinity and a_{CDOM} correlations of individual cruise, followed by their seasonal variations.

3.1.1. Salinity and a_{CDOM} Relationships of Different Cruises

[16] In general, salinity and $a_{CDOM}(355)$ were well correlated for all nine cruises with correlation coefficients (R) greater than 0.85 ($p < 0.001$), except for the C973 spring cruise with R of 0.74 (Table 1). Good correlations were also found between salinity and a_{CDOM} at 400 and 412 nm, albeit with slightly lower R and higher standard deviations (SD) than those at $a_{CDOM}(355)$. The regression results for $a_{CDOM}(400)$ were also better than those for $a_{CDOM}(412)$ (Table 1). Therefore, it appears that the shorter wavelength of a_{CDOM} was more appropriate for salinity inversion, as the nature of the exponential decay spectrum indicated. Here we focus on the analysis of a_{CDOM} at 355 nm, although the values at 400 and 412 nm are also used for comparison.

[17] The C908 cruises covered a full salinity range from freshwater to the Kuroshio water. For the regression of salinity and $a_{CDOM}(355)$, all C908 cruises had R values greater than 0.9 with SD values of 2–3 in the salinity unit. Among them, the summer cruise data showed the best correlation, with $R = 0.96$ and SD = 2.36. In addition, this data set also smoothly connected with that of the CCJE-Sept cruise located in the low-salinity regions (Figure 2a). Among the four C973 cruises, which were all located in higher salinity areas (>25), the SD was less than 1, except for the summer cruise, which had a slightly higher SD of 1.48. The C973 cruise data were also tightly clustered around the regression lines of the pooled C908 data, although some points deviated from the lines around salinities 28–32 (Figure 2b).

[18] The regression lines for the C973 cruises led to a much higher freshwater end-member because the data were located largely in high-salinity regions, while the regression line for CCJE-Sept alone led to a much lower marine end-member, with all of the data coming from the low-salinity regions (Figure 2c). These deviations indicate that, as may be expected, any extrapolation beyond the sampled data ranges may lead to large uncertainties. Thus, a general and robust salinity-a_{CDOM} relationship must be derived from the data set with a full salinity range.

3.1.2. Seasonal Variation of the Salinity-a_{CDOM} Relationships

[19] The differences between the individual cruises regression lines may largely reflect the seasonal variation of the salinity-a_{CDOM} relationship. In general, there were slight seasonal changes for the four regression lines from the C908 cruises. Such slight seasonal changes were also found in the C973 regression lines over the sampled salinity range (~25–34), except for the C973 spring cruise (Figure 2c).

[20] The in situ $a_{CDOM}(355)$ at the freshwater end-member (salinity near 0) was between 1.4 ~ 2.3 m^{-1} (Figure 2a). Showing by the seasonal regression lines of C908 cruises at salinities around 0 (Figure 2c), $a_{CDOM}(355)$ at the freshwater end-member increased from 2.1 to 2.4 m^{-1} from winter to spring, autumn, and summer, which was most likely controlled by the sequence of Changjiang River discharge from low to high [*Chen et al.*, 2008, 2009]. It is difficult to pinpoint the exact freshwater end-member value of a_{CDOM} due to the multibranching structure of the Changjiang Estuary, local metropolitan contamination, strong tidal effects, and likely seasonal variation in the upper stream source materials.

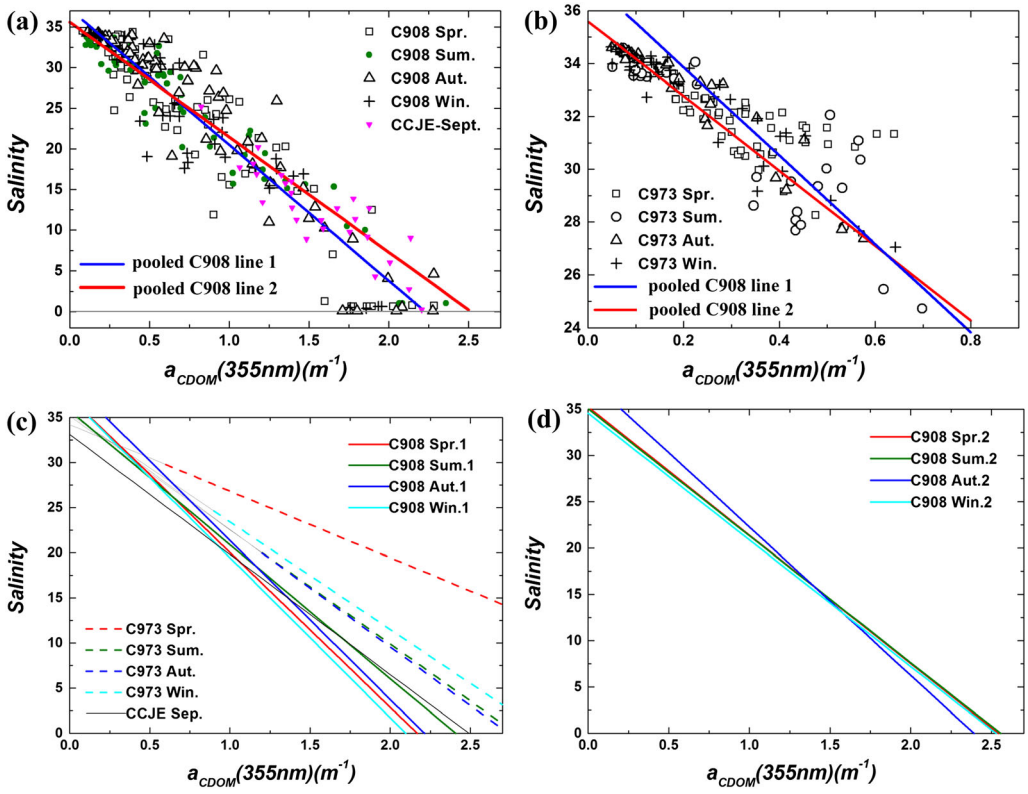

Figure 2. Relationships between salinity and $a_{CDOM}(355)$ in the Changjiang plume and surrounding ECS waters. (a) Data from four C908 cruises and the CCJE-Sept cruise. The blue solid line (line 1) is the regression line for the pooled C908 data, and the red solid line (line 2) is the regression line for the pooled C908 data with salinity ranging from 2 to 33, eliminating the variable river and marine end-member values. (b) Data from four C973 cruises with the regression lines for the C908 data. (c) Individual regression lines for the nine cruises with all measured data. To present a clear view, the regression lines for the four C973 cruises in high salinity have been replaced by thin gray lines. (d) Individual regression lines for four C908 cruises with salinity ranging from 2 to 33.

For the purpose of identifying a plume area, the freshwater end-member is fortunately not very critical. Although such discharge-dependent variation was small, further exploration is desirable and dependent on the availability of more data.

[21] For the marine end-member, $a_{CDOM}(355)$ varied at around 0.05–0.1 m^{-1} when the salinities were greater than 34.3 (Figures 2a and 2b). This was largely due to the mixing of multiple water masses on the outer shelf (e.g., the Taiwan Warm Current and Kuroshio water [*Yuan et al.*, 2008; *Chen*, 2009]). Although the marine end-member of a_{CDOM} was also hard to determine from the samples, this uncertainty did not affect our ability to identify the river plume.

[22] Instead of the direct regression of all of the measured data (the regression line marked as regression line 1 in Figure 2 and simply as "1" after the cruise time in Table 1), we limited the salinity range to 2–33 for the data from C908 cruises to develop the regression equations (the regression line marked as regression line 2 in Figure 2 and simply as "2" after the cruise time in Table 1), for the purpose of defining the freshwater plume and eliminating the influence of the variable end-member values. In general, regression line 2 had lower SD than regression line 1(Table 1). Without the effect of the freshwater end-member, regression line 2 had lower offset and higher slope than regression line 1 (Figures 2a and 2b). A comparison with the independent C973 data suggests that regression line 2 from the pooled C908 data was more appropriate for matching the high-salinity marine water than regression line 1, although regression line 2 slightly overestimated the salinity in the freshwater end-member (Figure 2b). This limitation is not a real problem for satellite-derived salinity mapping, because water with very low-salinity occupies only a very small area within and around a river mouth, and salinity increases very rapidly once the water exits an estuary.

[23] In Figure 2d, it is interesting to note that the regression line 2 from each individual C908 cruise were much closer to each other than the regression line 1, implying much smaller seasonal variation in the salinity-a_{CDOM} relationships in the majority of the salinity ranges. The regression line 2 from the autumn C908 cruise had higher modeled results than the regression line 2 from other seasons in the high-salinity region, perhaps due to the influence of phytoplankton blooms. This is similar to the regression line from the spring C973 cruise on which the blooms were encountered. We discuss these in section 4.2.

3.2. Comparison With Previous Studies

[24] To the best of our knowledge, four studies have shown the salinity-a_{CDOM} relationships in the ECS, including a study

by *Gong* [2004] of the southern ECS with four seasonal cruises from 1997 to 1998, a study by *Guo et al*. [2007] of the south branch of the Changjiang Estuary with one cruise in August 2003, and studies by *Sasaki et al*. [2008] and *Ahn et al*. [2008] of the northeastern ECS with data covering only the outer shelf (salinities all greater than 29). Because *Guo et al*. [2007] did not present a quantitative correlation equation for salinity and a_{CDOM}, we compare our regression results only with those of *Gong* [2004], *Sasaki et al*. [2008], and *Ahn et al*. [2008] with a_{CDOM} at 400 nm, because *Sasaki et al*. [2008] and *Ahn et al*. [2008] both used 400 nm as a reference wavelength. We also examine the robustness and generality of these salinity-a_{CDOM} relationships using our in situ data (Table 2 and Figure 3).

[25] Although the relationships between salinity and a_{CDOM}(400) were more scattered than those involving a_{CDOM}(355), based on our ECS data, all of the linear regression lines were generally quite similar, apart from some special cases (Figure 3). It is encouraging to find that three linear regression lines from (1) the low *chla* data of *Sasaki et al*. [2008], (2) the pooled data of *Ahn et al*. [2008], and (3) the pooled data of *Gong* [2004] were all approximately close to our pooled C908 regression line 2, although their slopes and offsets were different in the regression equations. This indicates that the linear relationship between salinity and a_{CDOM} is rather stable in the ECS, although their relationships have developed from different areas and seasons. In most cases, especially for the high-salinity marine water, our C908 regression line 2 data fit best with the C973 data.

[26] Note that it may not be appropriate to compare the data with the nonlinear equation of *Ahn et al*.'s [2008]. Although they preferred this exponential decay function, their equation seems to significantly overestimate the salinity. The apparent explanation is that their relationship may not be suitable for the ECS in the below-30 salinity range, because their equation was developed by combining the high-salinity data (greater than 30) from the ECS with low-salinity data from areas outside the ECS, such as Lake Ponchartrain and Mississippi Sound [*Miller et al*., 2002], where the a_{CDOM}(400) values were much higher than that of the Changjiang River freshwater. The regression line used by *Sasaki et al*. [2008], which was based only on data with *chla* greater than 1.3 μg/L, was approximately similar to that of the C973 in spring cruise. However, the regression lines created from data with high *chla* concentration only suit special cases. In addition, two algorithms (high-*chla* and low-*chla*) are not very practical when applied to a whole satellite image with a wide *chla* distribution.

3.3. Application to Satellite Ocean Color Data

[27] The accurate prediction of salinity in a plume area from ocean color satellite data requires a robust relationship to link salinity with a_{CDOM}, and that a_{CDOM} should be accurately retrieved from satellite-derived remote sensing reflectance. In the following subsections, a series of validations are presented to show the performances of the salinity-a_{CDOM} equation, satellite a_{CDOM} algorithms, and satellite-derived salinity mapping, with several in situ data sets.

3.3.1. Validation of the Salinity-a_{CDOM} Equation

[28] For the remote sensing application, the regression equation based on pooled C908 data with salinity ranging from 2–33 (regression line 2 from pooled C908) was used in the ECS:

$$SSS = 35.595 - 14.151 \times a_{CDOM}(355) \quad (3)$$

[29] The data from the four C973 cruises were taken as independent data sets to validate the model performance (Figure 4). Most of the model-derived data followed the 1:1 line well, with 73.6% of the data falling within the absolute salinity error of ±1, and 87.1% data falling within ±1.5. Overall, this result was sufficient for detecting the river plume with a large salinity gradient. The absolute errors of modeled salinity are displayed in the geographic maps for a clearer view of the deviations (Figure 5). In general, for most of the shelf area, the absolute errors of modeled salinity were within ±1, implying the good performance of our salinity model. Larger deviations were found in the highly turbid estuary and bays, especially the adjacent Hangzhou Bay in the southern Changjiang River Estuary, which was affected by strong tidal processes [*Su and Wang*, 1989; *Xie et al*., 2009]. Thus, it is appropriate to use the data with a 2–33 salinity range in

Table 2. Regression Results of Salinity and the Absorption Coefficient of Colored Dissolved Organic Matter (a_{CDOM}) at 400 nm From Literatures and Our Study[a]

	Salinity	a_{CDOM}(400)						
Cruises	(min-max)	(min-max)	Regression[a]	*N*	*A*	*B*	*R*	SD
Sasaki et al. [2008]	~(29–34)	~(0.05–0.26)	All	43	34.5	–19.5	–0.66	/ [c]
			chla < 1.3 μg/L	35	35.3	–27.3	–0.80	/
			chla ≥ 1.3 μg/L	8	33.9	–12.2	–0.91	/
Ahn et al. [2008]	(30–34.4)	(0.05–0.22)	Linear	24	36.655	–30.642	–0.93	/
			Non-linear[b]	37	35.064	–0.3357	–0.99	/
Gong [2004]	(/)	(0.017–0.444)	Spring	35	38.48	–40	–0.72	/
			Summer	34	35.947	–26.316	–0.9	/
			Autumn	34	36.969	–31.25	–0.78	/
			Winter	34	36.146	–20.833	–0.91	/
			All	137	36.636	–30.303	–0.78	/
This study C908all[d]	(0–34.52)	(0.08–2.36)	All	264	37.557	–34.637	–0.92	3.87
			Salinity(2-33)	192	35.599	–28.545	–0.86	3.49

[a]The linear regression equation is unified as $Salinity = A + B \times a_{CDOM}(400)$.
[b]The nonlinear regression equation of *Ahn et al*. [2008] is $Salinity = A \times e^{(B \times a_{CDOM}(400))}$.
[c]SD was not shown in the literatures.
[d]"C908all" indicated that the regression use the pooled C908 data from the four seasons.

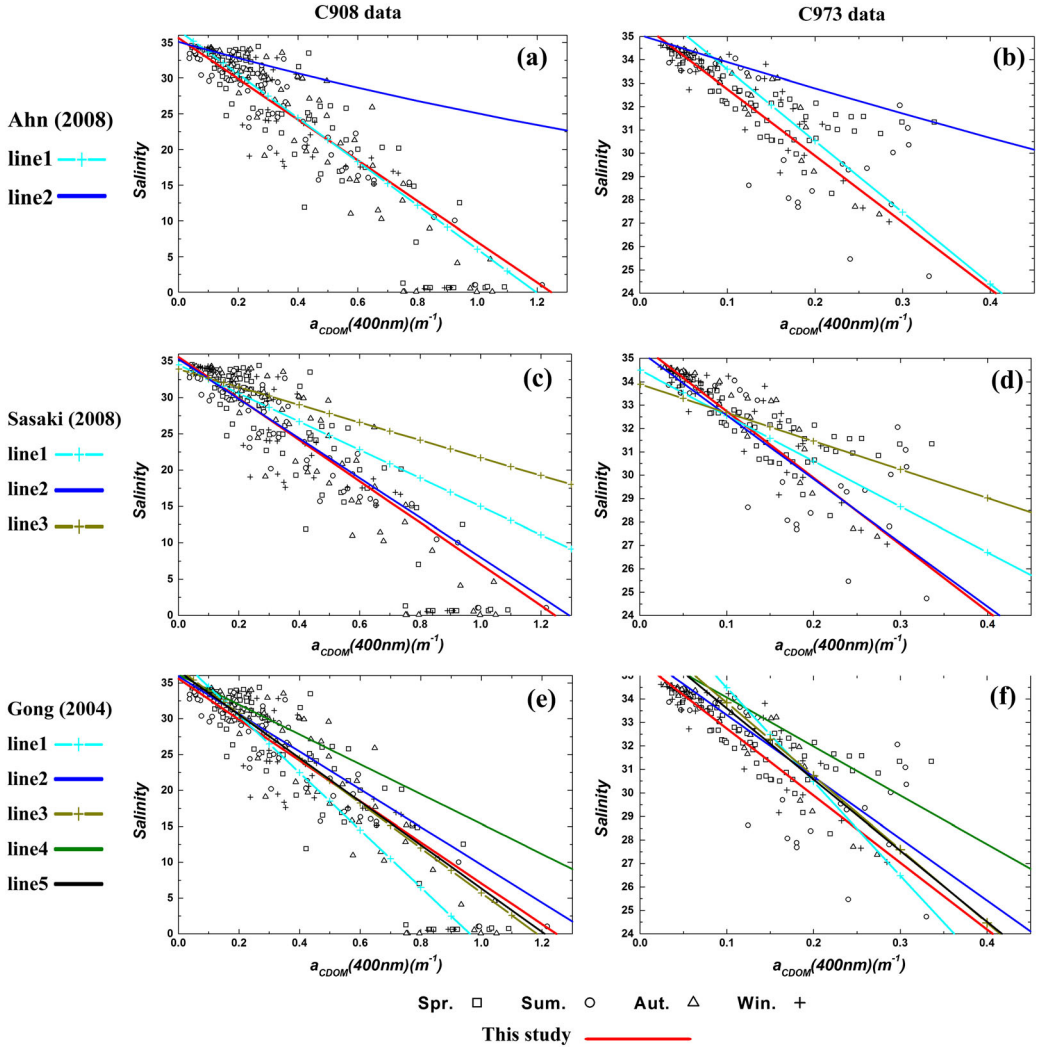

Figure 3. Regression lines of salinity and $a_{CDOM}(400)$ in this study (equation can be found in Table 1 and Table 2 with C908 all data with salinity from 2 to 33), *Sasaki et al.* [2008], *Ahn et al.* [2008], and *Gong* [2008]. Left-hand column shows the background of our in situ data during the C908 cruises, and right-hand column shows the data from the C973 cruise. For *Ahn et al.* [2008], line 1 and 2 are the linear and nonlinear regression lines (exponential function), respectively. For *Sasaki et al.* [2008], line 1 is the regression line from their pooled measured data, and lines 2 and 3 are from the data with *chla* < 1.3 μg/L and *chla* ≥ 1.3 μg/L, respectively. For *Gong* [2008], lines 1, 2, 3, 4, and 5 are the regression results from the cruises in spring, summer, autumn, winter, and their pooled data, respectively. The detailed equations of these three literatures can be found in Table 2.

the regression of equation 3 to avoid the freshwater with extremely high turbidity, which occupied only a very small area compared with the whole river plume.

[30] During the dry seasons of autumn and winter, most parts of the shelf had *chla* lower than 2 μg/L, and these areas had better modeled salinity results than the wet seasons of spring and summer. Some underestimations in autumn and winter were located at 32°N within the 50 m isobath, which was paralleled by a significant turbid tongue, induced by the southeastward flow from the Yellow Sea Coastal Current (YSCC) (Figure 1a) [*Yuan et al.*, 2008; *Yuan and Hsueh*, 2010]. A third end-member with higher CDOM from the turbid and well-mixed southeastward YSCC, rather than the Changjiang River, might have caused the underestimation of the modeled salinity.

[31] On the C973 spring cruise, stations with significantly underestimated salinities all had *chla* greater than 4 μg/L. These stations were located in a typical area experiencing frequent red tide occurrences [*Zhou et al.*, 2003; *Chen et al.*, 2007a]. The bloom-induced CDOM resulted in underestimation of the modeled salinity. These situations were more complicated in summer for the C973 and C908 cruises. Both underestimation and overestimation were found for *chla* greater than 2 μg/L. These results are discussed in section 4.2.

3.3.2. Validation of Satellite Algorithms for a_{CDOM}

[32] Because of the influence of rich terrestrial NAP, developing a satellite a_{CDOM} algorithm in the coastal oceans is a very challenging task [*Zhu et al.* 2011, and references therein]. As a first step toward the development of a new

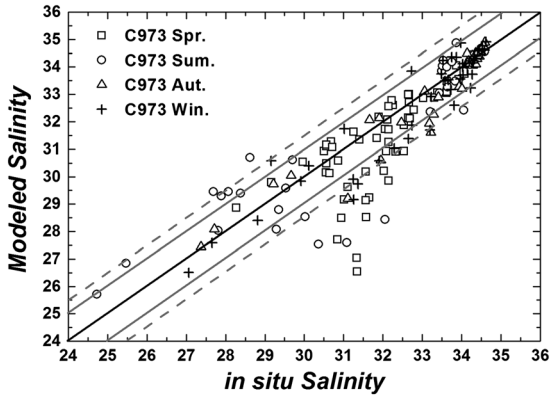

Figure 4. Validation result of modeled salinity based on the in situ salinity of the C973 data (total number = 163). The solid gray lines mark an absolute salinity error of ±1 with 73.6% of the data, and the dotted gray lines envelop 87.1% of the data within ±1.5.

a_{CDOM} algorithm for the ECS, we evaluated and validated three existing a_{CDOM} algorithms to show the ability of remote sensing to estimate salinity and detect plumes in the ECS.

[33] *Sasaki et al*. [2008] and *Ahn et al*. [2008] tried to map the Changjiang River plume with satellite ocean color data. The a_{CDOM} algorithm used by *Sasaki et al*. [2008] was exactly the a_{CDM} algorithm developed by *Carder et al*. [2003], who assumed that the a_{CDOM} was much greater than a_{NAP} on the outer shelf and thus $a_{CDOM} \approx a_{CDM}$. *Ahn et al*. [2008] developed a regional empirical algorithm for $a_{CDOM}(400)$, which was a power function of the ratio of $R_{rs}(412)/R_{rs}(555)$. In addition, *Zhu et al*. [2011] developed an extended QAA (QAA-E) algorithm to retrieve a_{CDOM} from QAA-derived a_{CDM} ($a_{CDOM} = a_{CDM} - a_{NAP}$) in the Gulf of Mexico. We evaluated these three algorithms with our ECS data sets (pooled C908 and C973 data).

[34] We validated $a_{CDOM}(400)$, because the algorithms of *Carder et al*. [2003] and *Ahn et al*. [2008] both retrieve a_{CDOM} at 400 nm. Because QAA-E retrieves a_{CDOM} only at the corresponding satellite sensor bands with the shortest band at 412 nm, for better comparisons with the two other products, we extrapolated the QAA-E derived a_{CDOM} values to the shorter wavelength at 400 nm, based on the estimates of spectral slope (S_{CDOM}):

$$a_{CDOM}(400) = a_{CDOM}(412)\exp[S_{CDOM} \times (412 - 400)]; \quad (4)$$

$$S_{CDOM} = \ln[a_{CDOM}(412)/a_{CDOM}(443)]/(443 - 412). \quad (5)$$

[35] For our in situ data sets, the $a_{CDM}(400)$ values from all three algorithms agreed with the measured data reasonably well in spring, summer, and autumn, although *Ahn et al*. [2008] predicted somewhat higher values than those of the other two algorithms (Figure 6). *Ahn et al*. [2008] also recognized this overestimation. We also caution our readers that a_{CDOM} in the study by *Carder et al*. [2003] is really a_{CDM}, which is supposed to be higher than a_{CDOM}.

[36] To determine a suitable algorithm for the ECS, we further validated and compared the a_{CDOM} algorithms of *Carder et al*. [2003] and *Zhu et al*. [2011] with two global data sets: (1) the IOCCG synthetic data at 30° zenith with the shortest wavelength at 400 nm, and (2) the global in situ NOMAD data (version 1.3) with the shortest wavelength at 405 nm, in addition to the data from our eight C908 and C973 cruises in the ECS. This time, we compared the inversed a_{CDOM} results at both the conventionally used 443 nm and the shortest wavelengths (355, 400, and 405 nm) of the in situ data sets. Although *Zhu et al*. [2011] tested their $a_{CDOM}(440)$ algorithm with IOCCG synthetic data, we further tested *Zhu_*a_{CDOM} at 400 nm, in addition to the a_{CDOM} at 405 and 355 nm with the in situ data of NOMAD and the ECS data sets. We extrapolated *Zhu_*$a_{CDOM}(412)$ to 405 and 355 nm with a method similar to that of 400 nm used in equations 4 and 5. In the algorithm of *Carder et al*. [2003], the S_{CDM} used to extrapolate a_{CDM} from the reference wavelength of 400 nm to the other wavelengths was a fixed value of 0.017 nm^{-1}, which may be somewhat higher in some regions [*Carder et al*., 2003].

[37] Figure 7 shows that both of the algorithms performed well for the IOCCG synthetic data sets, although the results of *Zhu_*a_{CDOM} is better than the *Carder_*a_{CDM}, with higher R and lower SD, because *Zhu et al*. [2011] adjusted the empirical coefficients based on this data set. For the global in situ data of NOMAD and our ECS data sets, it showed that *Carder_*a_{CDM} performed better in general with higher R, lower SD, and more valid values than *Zhu_*a_{CDOM}, although the inversed a_{CDOM} from both algorithms was scattered and not particularly satisfactory. Future improvements of the a_{CDOM} algorithms are still required for the ECS.

[38] We achieved another useful result from this validation. The performance of the a_{CDOM} inversion at the shortest extrapolated wavelength was better than that at the conventionally used 443 nm. Although the extrapolation introduced new uncertainty around the selection of the S_{CDOM} value, this uncertainty can be compensated by the good side of a larger a_{CDOM} value at shorter wavelengths with lesser influence by other materials (phytoplankton and detritus). We discuss this further in section 4.3.

3.3.3. Mapping the Salinity by Satellite Ocean Color Data

[39] Using the salinity-$a_{CDOM}(355)$ relationship and the $a_{CDOM}(355)$ inversed by the algorithm of *Carder et al*. [2003], we generated daily satellite-derived salinity maps in the ECS from the daily $R_{rs}(\lambda)$ products of MODIS/Aqua. Due to heavy cloud cover in the ocean color data, there were fewer match-up data between the in situ measurement and the daily satellite-derived salinity products. As such, we generated a 16 day composite satellite salinity map during the C973 cruise in the ECS (16–30 August 2009) (Figure 8a). Then, we compared the satellite-derived salinity with the in situ underway salinity data collected during the cruise (Figure 8b). Although there were large temporal and spatial gaps between the underway measurements (1 min measuring period and a single point location) and the salinity map (16 day average and $4 \times 4\ km^2$), the comparison results were encouraging, and these two measures provided a sufficiently matched data set for evaluating the satellite inversion and plume detection capability.

[40] In general, the satellite results showed similar fluctuation with the in situ data, and this presented a good synoptic view of the distribution of the low-salinity Changjiang River plume (Figures 8a and 8b). As shown in Figure 8a, the

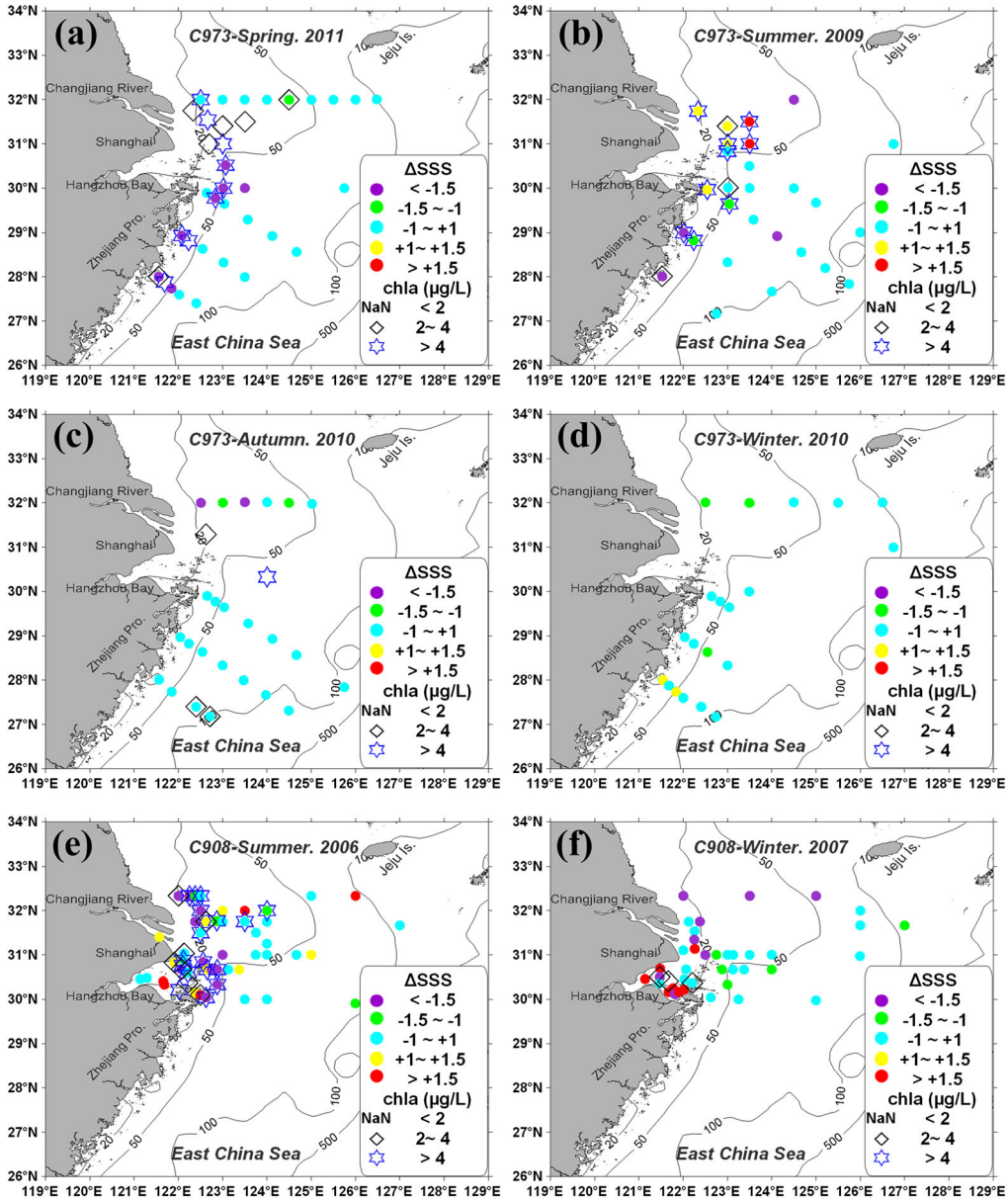

Figure 5. Absolute error between modeled salinity and in situ salinity (marked Δ*SSS*). (a–d) Data from the four C973 cruises, and (e–f) data from the C908 cruises in summer and winter. Lacking the *chla* data, the figures from the spring and autumn C908 cruises were not shown. *chla* concentrations are marked by different symbols overlaying the modeled salinity errors.

low-salinity Changjiang River plume extended to the northeast after leaving the estuary, and reached Cheju Island. This is the normal movement of low-salinity water under the prevailing southwest monsoon during summer [*Moon et al.*, 2009]. In addition, the satellite image also provided a vivid view of a rare low-salinity tongue intruding into the middle shelf at ~29°N. This low-salinity tongue was also caught by the underway measurements on 22 August, but in a very limited area (Figure 8b). This southeastward extending low-salinity tongue was a notably episodic event induced by typhoon Morakot (a category 2 typhoon), which first landed on eastern Taiwan Island on 7 August 2009 and then landed in Fujian Province on 9 August. The strong cyclone lasted for several days, halted the typical northward coastal current in summer, and triggered the southeastward current (*He et al.*, Cyclone-driven terrestrial material transport to the Okinawa Trough: Direct satellite observations, submitted to *Journal of Marine Systems*, 2012).

[41] To further evaluate the applicability of the salinity inversion algorithm, we also generated monthly-composite satellite-derived salinity images in August from 2008 to 2010 based on our salinity-a_{CDOM} equation and the a_{CDOM} (355) algorithm of *Carder et al.* [2003] (Figure 9). It appears that the algorithm was able to catch the significant interannual variations of the Changjiang River plume, which was smallest in 2009, moderate in 2008, and largest in 2010. These results are nearly consistent with the Changjiang River discharge amount of 36,947 m^3/s, 39,574 m^3/s, and 54,274 m^3/s (monthly-mean value from June to August) for 2008, 2009, and 2010, respectively (discharge data taken from Datong

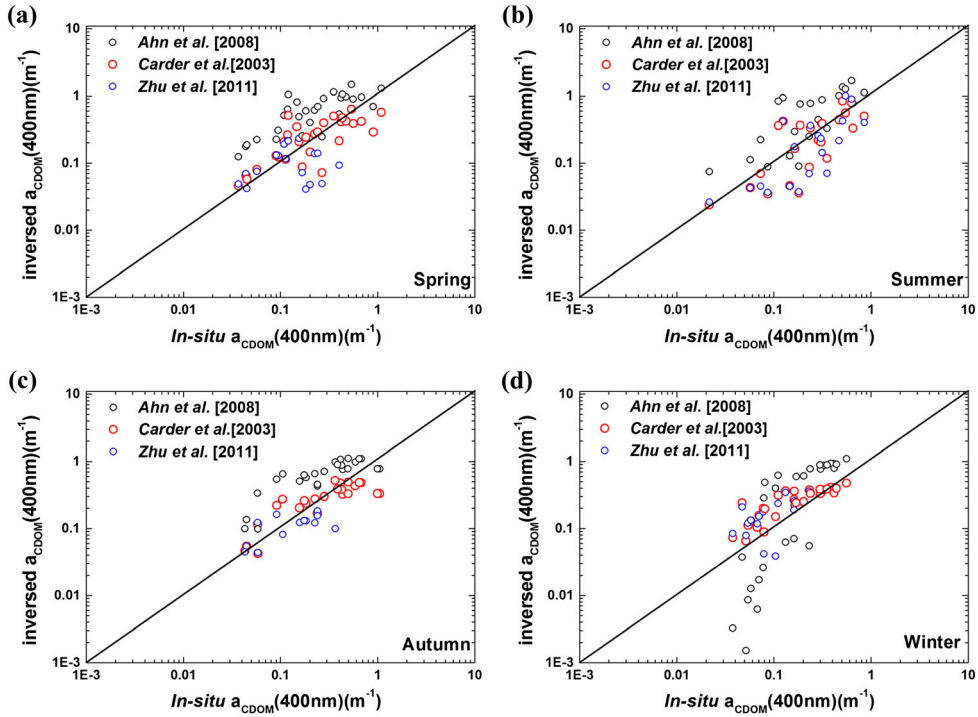

Figure 6. Validation results of three algorithms of $a_{CDOM}(400)$ based on the four seasonal in situ data from the C908 and C973 cruises in the ECS. Note that the algorithm needs the input of in situ $R_{rs}(\lambda)$, which must be measured in the daytime. Therefore, the total number of valid samples in the ECS was much less than the number of water samples for CDOM. For *Carder et al.* [2003], the inverse results were actually the a_{CDM}, which was used considered as a_{CDOM}.

hydrological gauging station, http://www.hydroinfo.gov.cn). The plume area was extremely large in 2010, when the discharge was almost at its highest in the recent decades. This result implied that one of the most important factors regulating the plume area is the river discharge, and satellite data can provide a valuable tool for examining how flood events influence coastal ocean dynamic and biogeochemical processes, which are difficult to assess from limited field surveys.

[42] We recognize that in such a highly dynamic plume system, some deviations between the 16 day composite satellite map and the in situ data were unavoidable. Some deviations were still larger than we would have liked. In addition to the temporal and spatial gaps between these two matched data sets, deviations also resulted from many steps required to process the satellite data. We discuss this in section 4.4.

4. Discussion

4.1. Factors Influencing the Salinity-a_{CDOM} Relationship

[43] The principles behind the salinity inversion from a_{CDOM} in coastal oceans are based on the conservative behavior of CDOM and the overwhelming physical mixing between freshwater and marine water with distinct CDOM values and features. *Bowers and Brett* [2008] suggested that a linear relationship can be expected in an estuary if the river discharge and CDOM concentration vary on time scales longer than the flushing time of the estuary. As the fourth largest river in the world in terms of discharge, the Changjiang River Estuary has a rapid flushing time (i.e., a few days [Zhang *et al.*, 2007]). Thus, a linear correlation between salinity and a_{CDOM} in the low-salinity area is expected even though the Changjiang River discharge and terrestrial CDOM concentration vary seasonally and sometimes episodically.

[44] In addition to the physical mixing, however, there are a number of chemical and biological processes that influence the distribution and optical properties of CDOM in the plume area [*Blough and Del Vecchio*, 2002]. These include the autochthonous production of CDOM from degradation of phytoplankton and bacteria [*Nelson et al.*, 1998, 2010; *Twardowski and Donaghay*, 2001; *Stedmon and Markager*, 2005], photochemical bleaching [*Chen et al.*, 2004], and sediment resuspension [*Boss et al.*, 2001].

[45] The most important removal process of CDOM is photooxidization (photobleaching). However, noticeable CDOM removal usually takes weeks to months [*Vodacek et al.*, 1997], such as a case in Tampa Bay, where the removal was conducted under strongly stratified conditions with a long residence time of the water mass [*Chen et al.*, 2007b]. In the case of the Changjiang River plume, although stratification occurs due to the freshwater buoyancy, especially in summer, the huge river discharge and short residence time limit the photobleaching. In addition, vertical mixing and high turbidity further limit the photobleaching in the tidal estuary and the inner shelf in the dry seasons. *Guo et al.* [2007] also found that CDOM behaved conservatively in the Changjiang Estuary and that no significant photobleaching removal occurred in the high-salinity region.

[46] The influence of biological processes on CDOM is another important consideration during salinity inversion, and we discuss it in more detail in the next subsection.

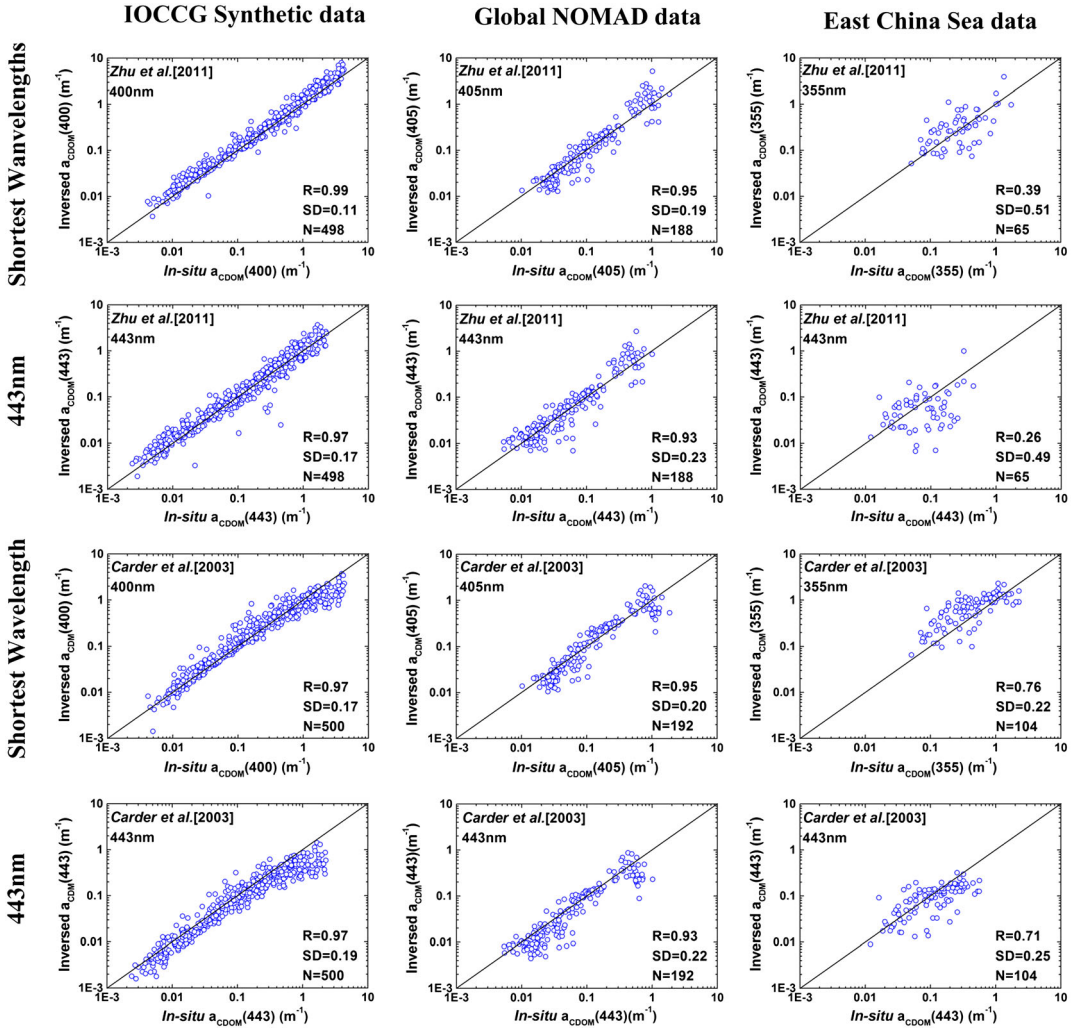

Figure 7. Validation results of three a_{CDOM} algorithms based on several in situ data sets with the black 1:1 line. Columns 1–3 are data from the Global IOCCG synthetic data at 30° zenith, the global data from NOMAD (version 1.3) and data from C908 and C973 cruises in the ECS, respectively. Rows 1 and 2 are the a_{CDOM} at its shortest wavelength and the conventional 443 nm, respectively, retrieved by the algorithm of *Zhu et al*. [2011]. Rows 3 and 4 were retrieved using the algorithm of *Carder et al*. [2003].

Because we have achieved a reasonable linear regression between salinity and a_{CDOM} with our abundant data sets, including those with expected biological effect, we argue that the autochthonous input is not a major controlling factor on CDOM in the ECS overall. This notion is consistent with the argument of *Twardowski et al*. [2004] that the in situ production of CDOM in terrestrially dominated waters may be evident only under a relatively stable water mass containing a high level of phytoplankton but a relatively low background of terrestrial CDOM. *Chen et al*. [2009] found a low production-to-respiration ratio in the ECS plume waters, suggesting the dominance of allochthonous organic matters over in situ biological production. Moreover, terrestrial CDOM absorbs light strongly in ultraviolet bands due to its tannins and lignin [*Hernes and Benner*, 2003] and because it has a different optical character than marine CDOM, which has few aromatic rings and absorbs weakly at 350 nm [*Helms et al*., 2008; *Palacios et al*., 2009]. Therefore, the CDOM at the ultraviolet bands contains more terrestrial features, which would weaken the influence of the autochthonous CDOM from phytoplankton and bacterial production on the salinity-a_{CDOM} relationship.

[47] In general, because photobleaching and biological processes that change CDOM concentrations typically occur on time scales that are longer than water transit period, they are commonly masked by the direct physical mixing between the terrestrial and marine CDOM signals in large river-influenced systems [*Blough and Del Vecchio*, 2002; *Hitchcock et al*., 2004; *Bowers and Brett*, 2008]. The good, linear, and nearly stable relationship between salinity and a_{CDOM} found in our study, in addition to similar regression equations from *Gong* [2004], *Sasaki et al*. [2008] and *Ahn et al*. [2008], support this general notion.

4.2. The Effect of Autochthonous CDOM on Salinity Inversion

[48] Phytoplankton blooms are found regularly in the Changjiang River plume during spring and summer, when

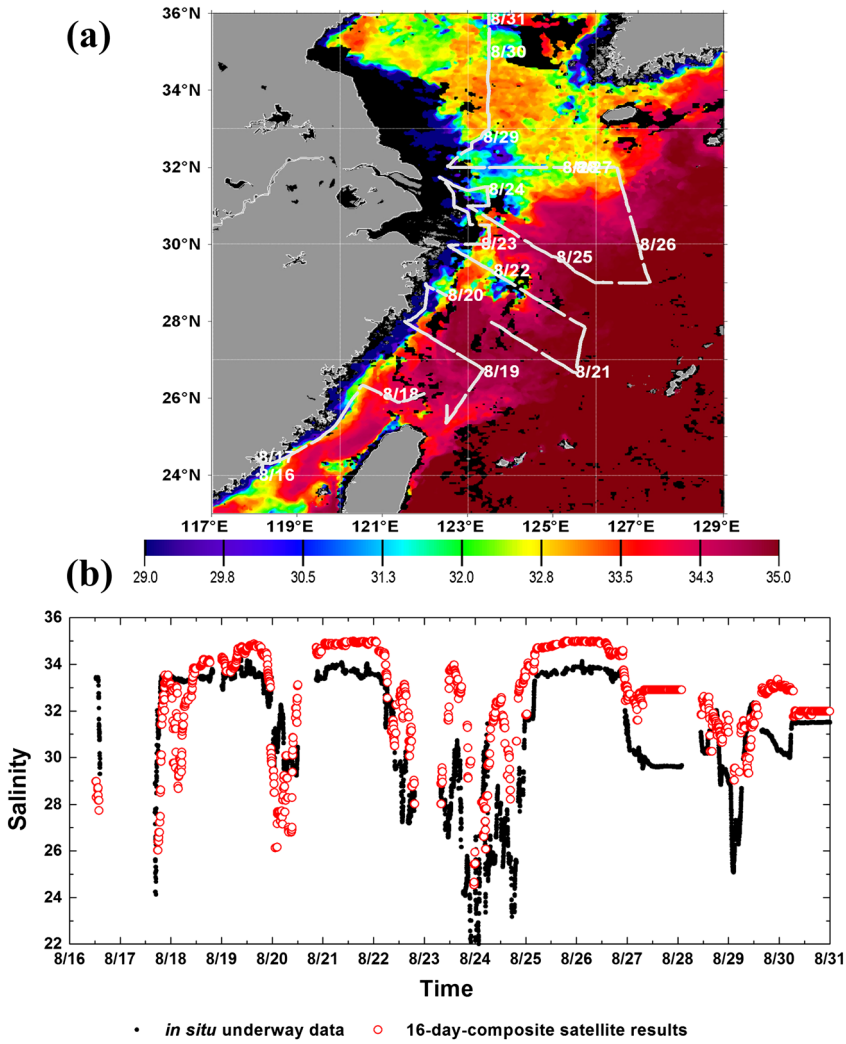

Figure 8. Comparison between the satellite-derived salinity and the in situ underway measures. (a) The cruise track during 16–31August 2009 with the background of the 16 day composite satellite map during the cruise. The black color indicates invalid data masked by clouds and highly turbid water. (b) Point-to-point comparison between the in situ data and the satellite-derived salinity based on the $a_{\mathrm{CDOM}}(355)$ algorithm from *Carder et al.* [2003]. Note that the time windows of the underway measurement and satellite data were 1 min and a 16 day average, respectively.

the river carries a high terrestrial nutrient load and has suitable light and temperature conditions [*Isobe and Matsuno*, 2008; *Chen et al.*, 2009; *Gong et al.*, 2011]. Phytoplankton blooms can increase CDOM under bloom conditions compared with nonbloom conditions [*Zhao et al.*, 2009]. In consequence, such autochthonous CDOM additions can alter the CDOM conservative behavior and result in lower modeled salinity, as was observed in the bloom events during the spring and summer cruise of C973 (Figure 4).

[49] Although some studies have tried to identify CDOM sources [*Twardowski and Donaghay*, 2001; *Stedmon and Markager*, 2001; *Murphy et al.*, 2008; *Helms et al.*, 2008], it is still difficult (or impossible at present) to separate the absorption signal of terrestrial CDOM from that of autochthonous CDOM ($a_{\mathrm{CDOM@phy}}$) in satellite ocean color data. Here we attempt to assess the influence of $a_{\mathrm{CDOM@phy}}$ on the salinity inversion. We assume that $a_{\mathrm{CDOM@phy}}$ in the outer shelf water is negligibly influenced by the terrestrial input and is similar to that in the open ocean (the so-called Case 1 water). As the Case 1 water definition [*Sathyendranath*, 2000] indicates, phytoplankton is the principal agent responsible for variations in the optical properties of the water; thus, it is also stipulated that the contribution from other substances (CDOM and NAP) is relatively small and that their optical properties can be modeled as a function of phytoplankton concentration. Therefore, we used the following equation to model the total absorption coefficients:

$$a(\lambda) = \left[a_w(\lambda) + 0.06 \times a^*_{chla}(\lambda) \times C^{0.65}\right] \times \left[1 + 0.2 \times a_{\mathrm{CDOM}}(\lambda)\right] \quad (6)$$

where C is the *chla* concentration; $a^*_{chla}(\lambda)$ is the specific-*chla* absorption coefficient; and $a_{\mathrm{w}}(\lambda)$ is the absorption coefficient of pure water. Equation 6 and the values of $a^*_{chla}(\lambda)$ and $a_{\mathrm{w}}(\lambda)$ were taken from *Morel and Gentilli* [1991] and *Prieur and Sathyendranath* [1981]. Thus, we had the following equation on the a_{CDOM} at 440 nm:

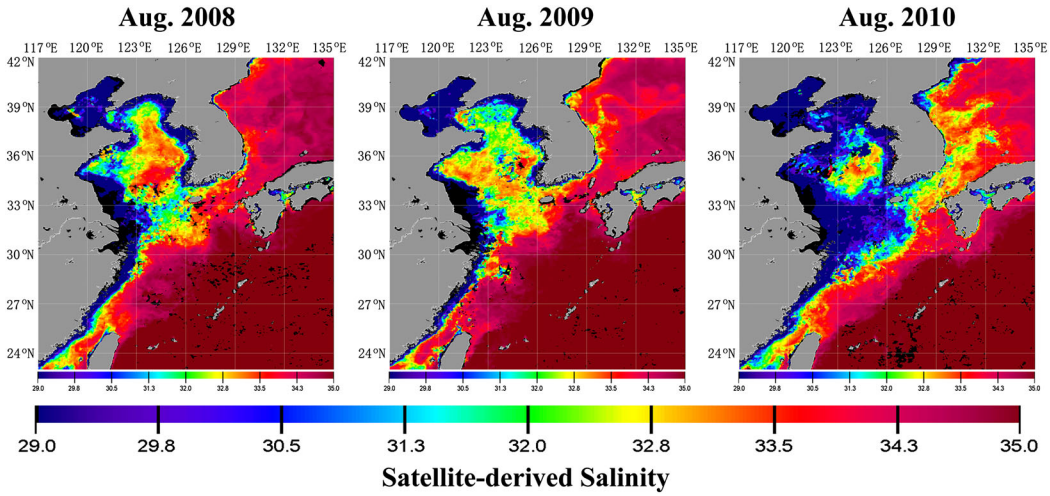

Figure 9. Monthly averaged satellite-derived salinity maps in August during 2008–2010, based on $a_{CDOM}(355)$ inversed by the *Carder et al.* [2003] algorithm.

$$a_{CDOM@phy}(440) = 0.003 + 0.012 \times C^{0.65}, \quad (7)$$

Then, $a_{CDOM@phy}$ at 355 nm could be extrapolated from 440 nm:

$$a_{CDOM@phy}(355) = a_{CDM@phy}(440) \times \exp[0.014 \times (440 - 355)]; \quad (8)$$

With equation 7 and equation 8, we obtained

$$a_{CDOM@phy}(355) = 0.009861 + 0.039445 \times C^{0.65}. \quad (9)$$

Therefore, the underestimation of salinity (ΔSSS) caused by the addition of phytoplankton-induced CDOM, $a_{CDOM@phy}$, was estimated from equation 3 based on the linear relationship between salinity and $a_{CDOM}(355)$

$$\Delta SSS = B \times a_{CDOM@phy}(355) = B \times \left(0.00986 + 0.03944 \times C^{0.65}\right), \quad (10)$$

where B is the slope of the regression equation between salinity and a_{CDOM} (Table 1). For our equation 3, B was 14.1505.

[50] Equation 10 shows that ΔSSS caused by $a_{CDOM@phy}$ is less than 1 when $chla \leq 2$ µg/L, and less than 1.5 when $chla \leq 4$ µg/L. Even with a *chla* concentration up to 10 µg/L, ΔSSS is still less than 2.6 (Figure 10). Therefore, phytoplankton blooms in the nutrient-rich plume area have only a limited influence on plume area detection. In addition, the patchiness of blooms can further limit the influence in the whole salinity field.

[51] Equation 10 can also be considered as a possible approach to correct the modeled salinity underestimates. Therefore, we used the in situ data of salinity, a_{CDOM}, and *chla* from the C973 cruises to explore this approach. From Figure 11a, it is clear that the modeled salinities that were significantly lower than the in situ salinities occurred largely in areas with high *chla* concentrations. After adding the ΔSSS estimated from equation 10 back to the original modeled salinity, the corrected salinities agreed much better with the in situ data along the 1:1 line (Figure 11b). For the 50 underestimated data, the averaged absolute error of salinity

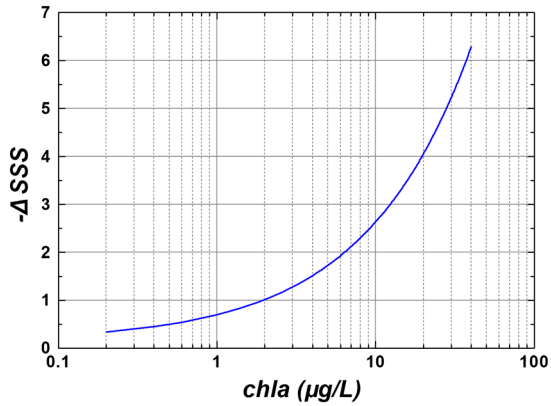

Figure 10. Underestimated salinities (ΔSSS) vary with the increase of *chla* concentration based on the bio-optical model of equation 10. $\Delta SSS < 1$ when $chla \leq 2$ µg/L, $\Delta SSS < 1.5$ when $chla \leq 4$ µg/L, and $\Delta SSS = 2.6$, when $chla = 10$ µg/L.

was 1.58 before *chla* correction, and it reduced to 0.94 after the correction. These results supported the correcting applicability of equation 10.

[52] Bearing in mind that the in situ situation is very complicated, equation 10 only considers the situation in which a positive correlation exists between a_{CDOM} and *chla* in the phytoplankton growth stage; it is not suited for the dissipation and degradation stage. In Figure 11a, it is noted that even in significant phytoplankton blooms with $chla > 10$ µg/L, all three cases occurred with modeled salinities that underestimate or overestimate or agree with the observations, although most deviations are toward an underestimation, as one may expect. Such an inconsistency is not totally unexpected. *Nelson et al.* [1998] and *Hu et al.* [2006] suggested that a_{CDOM} was not correlated with *chla* concentration and phytoplankton pigments, because CDOM was not the direct product of phytoplankton photosynthesis, but rather the product of microbial decomposition. Thus, the seasonal variation of CDOM in the open ocean is different from the growth cycle of phytoplankton. *Hu et al.* [2006] found that CDOM peaks and troughs followed the phytoplankton pigment cycle

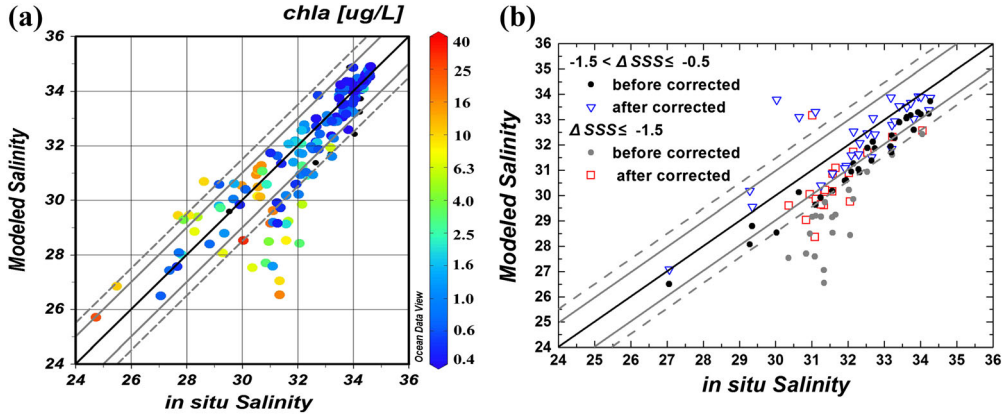

Figure 11. Validation and correction of the effect of phytoplankton blooms on the salinity inversion with the pooled C973 data. (a) Plot with the in situ *chla* concentration marked by color. (b) Correction of the modeled salinity based on equation 10. Note that only the underestimated data with $\Delta SSS \leq -0.5$ in Figure 11a are corrected in Figure 11b.

on delays of approximately 2 and 4 weeks, respectively. Therefore, different biogeochemical processes at diverse time scales further complicate the a_{CDOM}-*chla* relationship. This complication increases the difficulty of correcting autochthonous CDOM in the salinity model. Further data and studies are needed to provide deeper insight into a_{CDOM} variations and to further improve the salinity inversion model.

4.3. Selection of the a_{CDOM} Reference Wavelength

[53] We prefer to use 355 nm as the reference wavelength of a_{CDOM} to develop the algorithm for satellite-derived salinity. Our results and previous studies provided three reasons for using this approach. First, due to the nature of the exponential decay spectrum, a_{CDOM} has a stronger signal and lower sensitivity to other materials (detritus and phytoplankton) at shorter wavelengths compared with longer wavelengths. As shown by our regression and validation results, $a_{CDOM}(355)$ performed better than a_{CDOM} at the longer wavelengths (i.e., 400 and 412 nm). Second, the ultraviolet wavelengths of a_{CDOM} have more terrestrial signals than the blue wavelengths. *Hernes and Benner* [2003] found that a_{CDOM} at ~350 nm had strong correlations with dissolved lignin, an unambiguous tracer of terrestrial vascular plant sources. Third, 355 nm is used in most biogeochemical studies of CDOM, because it coincides with the pulsed frequency used in shipborne and airborne laser fluorescence spectroscopy sensing [*Berto et al.*, 2010]. Thus, using 355 nm can also be of direct help to biogeochemical research.

[54] The biogeochemical studies of CDOM optical properties have shown no uniform reference wavelength. To obtain stronger signals, some studies used wavelengths shorter than 355 nm, such as 325 nm [*Nelson et al.*, 2010] and 300 nm [*Stedmon et al.*, 2010]. Even shorter wavelengths were used to investigate the terrestrial features of CDOM. For example, *Berto et al.* [2010] used 280 nm as the spectral region in which aromatic substances, which are mainly substances of terrestrial origin, such as lignin, absorb. *Helms et al.* [2008] and *Fichot and Benner* [2011] used 275 and 295 nm as proxies for the molecular weight of dissolved organic matter and thus for the retrieval of the dissolve organic carbon (DOC) concentration from a_{CDOM}. However, for remote sensing applications, we believe that wavelengths shorter than 355 nm are not appropriate, due to the different S_{CDOM} at ultraviolet wavelengths and the elevated risk of long distance extrapolation from the common band of ocean color sensors. Thus, 355 nm is the preferred wavelength for developing the satellite-derived salinity algorithm.

4.4. Improvement of the Satellite a_{CDOM} Algorithm

[55] From the three validation steps in section 3.3 (the salinity-a_{CDOM} equation, the satellite a_{CDOM} algorithms, and the final satellite-derived salinity data), we know that the major errors of satellite salinity data are mainly propagated from satellite-derived a_{CDOM} errors. Thus, the biggest challenge in satellite-derived salinity mapping is the accurate retrieval of a_{CDOM} from satellite ocean color data in coastal waters. This involves several complicated processes, such as the retrieval of $R_{rs}(\lambda)$ from the atmospheric correction algorithm [e.g., *He et al.*, 2004; *He et al.*, 2012; *Wang et al.*, 2007] and the retrieval of $a_{CDOM}(\lambda)$ from the bio-optical model [e.g., *Lee et al.*, 2002; *Zhu et al.*, 2011]. Errors in each step are propagated into the final results; therefore, more effort should be made to improve the satellite a_{CDOM} algorithm in coastal waters.

4.4.1. Overestimation in the Marine End-Member

[56] The a_{CDOM} algorithms of *Carder et al.* [2003] and *Zhu et al.* [2011] both overestimated salinity in the marine end-member. This common result implies that the problems may arise from (1) deviation from the satellite-derived $R_{rs}(\lambda)$, and (2) altered marine end-members in summer.

[57] We found that the lowest in situ $a_{CDOM}(355)$ values were all greater than 0.05 m^{-1}, while the lowest satellite-derived $a_{CDOM}(355)$ was about 0.04 m^{-1}. *Sasaki et al.* [2008] also found that the $a_{CDM}(400)$ values were underestimated from the algorithm of *Carder et al.* [2003]. To correct this problem, *Sasaki et al.* [2008] established a multiple regression equation with the satellite-derived $a_{CDM}(400)$ and *chla*. Although this was a practical way of tackling the problem, we feel that such an empirical equation developed from limited data set may be vulnerable. Further data are required to identify the reasons for such underestimation and accomplish a more accurate correction.

[58] An altered marine end-member can also contribute to this issue. In the summer of 2009, the measured salinity of the marine end-member was 33.2–34, which was lower than

that in the autumn and winter seasons (~34.5). This lower marine end-member was probably the combined result of a greater river discharge during summer and a seasonal variation in the position of the Kuroshio Current, making the surface layer salinity in the outer shelf a little bit lower in summer (Kuroshio out-ward) than in winter (Kuroshio shelf-ward) [*Chen*, 2008; *Liu and Gan*, 2012]. Therefore, a proper correction method should be established to adjust this variation.

4.4.2. Improvement of the QAA-E a_{CDOM} Algorithm

[59] We showed the good performance of satellite-derived salinity images with the a_{CDOM} algorithm of *Carder et al*. [2003] in summer, the season with the largest Changjiang River discharge and greatest plume stratification due to the buoyancy of freshwater. In the wet seasons, particles settle very fast after water leaves the turbid maximum zone in the estuary. Thus, the water in the river plume is relatively clean, and the effect of suspended sediment on an a_{CDOM} algorithm can be ignored. However, in the dry seasons, because of strong vertical mixing and thus high particle concentration, the accuracy of the a_{CDOM} algorithm is degraded under the influence of high $a_{NAP.}$ Therefore, improvement of the a_{CDOM} algorithms is required in the next step.

[60] *Carder et al*.'s [2003] algorithm retrieves a_{CDM}, but not a_{CDOM}. Although the final inversed salinity from *Carder*_a_{CDM}(355) showed better performance in our study, it actually may not be the proper algorithm for a_{CDOM} retrieval in further studies. The good performance of *Carder*_a_{CDM}(355) might result from two compensations. First, *Carder*_a_{CDM}(355) slightly overestimates the in situ a_{CDOM}(355) at the algorithm level (seen in Figure 7), which would compensate the underestimation of satellite-derived a_{CDOM}(355) from satellite-derived $R_{rs}(\lambda)$. Second, a_{CDOM} is often overestimated in satellite data processing under the influence of high a_{NAP}, but this would be compensated by the significant underestimation of *Carder*_a_{CDM}(355) in coastal waters.

[61] We prefer the quasi-analytical algorithm based on the idea of separating a_{CDOM} from a_{CDM}. Although there are some challenges involved with the QAA-E algorithm [*Zhu et al*., 2011] in its current form, such a quasi-analytic algorithm has promising room to improve with more accurate parameterization for bio-optical models. Further effort should be made to improve the a_{CDOM} algorithm locally in the ECS by eliminating the particle influence, especially for the turbid dry seasons. We need to further examine the CDOM spectrum and the spectral slope (S_{CDOM}) and evaluate the contribution of NAP and CDOM to the total absorption coefficient in the quasi-analytic bio-optical algorithm.

5. Conclusions

[62] This study developed a good linear relationship between salinity and a_{CDOM} in the Changjiang River plume-dominated ECS based on nine cruises, covering all of the seasons and the complete salinity range. The relationship is robust and generalized, as supported by validation results from independent data sets and comparison with the salinity-a_{CDOM} regression equations from previous studies, developed in various areas of the ECS. Due to the prevailing physical water transport process, salinity-a_{CDOM}(355) relationship is less influenced by biogeochemical processes. We generated satellite-derived salinity maps for the less turbid summer season, which presented a good synoptic view of the plume area. The current work provides a good basis for a more robust and general satellite algorithm for a_{CDOM} in the ECS in the future. This approach for creating a satellite-derived salinity algorithm will enable us to examine the interannual variability of the river plume and its associated biogeochemical properties. It will also be useful in the development of satellite algorithms for salinity-dependent biogeochemical parameters, particularly the inversion of the aquatic partial pressure of CO_2 (pCO_2) in the river plume (Bai, in preparation, Remote sensing of coastal-ocean aquatic pCO_2 using a mechanistic-based semi-analytic method and a case study in the East China Sea).

[63] The satellite data from multiple sensors (ocean color and microwave) offer accumulating information of the dynamic salinity field and water mass movements. *Reul et al*. [2009] demonstrated the salinity measurements from space over theAmazon plume with the C- and X-band data from the Advanced Microwave Scanning Radiometer - Earth Observing System. The newly orbiting microwave sensors of SMOS and Aquarius (L-band radiometers) specially designed for the global salinity field can provide the open ocean surface salinity data with a high accuracy of 0.2. However, for the highly dynamic plume regions in coastal oceans, ocean color sensors (e.g., SeaWiFS and MODIS) still have the merits of higher spatial resolution (typically about 1 km) and frequent observation (once or twice per day). With the new generation of ocean color sensors, spatial and temporal resolutions can further improve. The world's first geostationary satellite ocean color sensor, Geostationary Ocean Color Imager, was launched in 2010 and has 500 m spatial resolution, 1 h temporal resolution (eight images per day), and particularly covers the coasts of East China, the Korean peninsula, Japan and the corresponding shelves and open oceans [*Ryu et al*., 2011; He et al., Using geostationary satellite ocean color data to map the diurnal dynamics of suspended particulate matter in coastal waters, submitted to *Remote Sensing of Environment*, 2012]. It will be very useful for monitoring the diurnal dynamic of the Changjiang plume. Taking advantage of both ocean color and microwave sensors, the synergistic use of these two technologies will further strengthen our ability to understand plume dynamics in coastal ocean biogeochemical research [*Salisbury et al*., 2011].

[64] **Acknowledgments.** This work was supported by the National Basic Research Program of China ("973" Program, grant 2009CB421202), the Public Science and Technology Research Funds Projects of Ocean (grant 200905012), the National Natural Science Foundation of China (grant 41271378, 40976110 and 41271417), and the National High-Tech Research and Development Program of China grants ("863" Program) (grants 2007AA092201 and 2008AA09Z104). We appreciate the people who worked on the cruises and in the laboratory. In particular, we thank Daji Wang and Zhiliang Liu for providing salinity data from the 908 Project and 973-CHOICE-C Project, respectively; Weidong Zhai for providing the underway salinity data from the summer cruise of the 973 Project; and Jun Sun for providing the chlorophyll *a* concentration data from the 973 Project. We thank NASA for providing the MODIS satellite data and the NOMAD in situ data and for making the data available systemically, and the Ministry of Water Resources of the Peoples' Republic of China for providing the Changjiang River discharge data. We also thank D. G. Bowers and the other two anonymous reviewers for providing valuable comments, which helped strengthen the manuscript.

References

Ahn, Y. H., P. Shanmugam, J. E. Moon, and J. H. Ryu (2008), Satellite remote sensing of a low-salinity water plume in the East China Sea, *Ann. Geophys.*, *26*, 2019–2035.

Berto, D., M. Giani, F. Savelli, E. Centanni, C.R. Ferrar, and B. Pavoni (2010), Winter to spring variations of chromophoric dissolved organic matter in a temperate estuary (Po River, Northern Adriatic Sea), *Mar. Environ. Res.*,*70*,73–81.

Binding, C. E., and D. G. Bowers (2003), Measuring the salinity of the Clyde Sea from remotely sensed ocean colour, *Estuarine, Coastal and Shelf Sci.*, *57*, 605–611.

Blough, N. V., and R. Del Vecchio (2002), Chromophoric DOM in the Coastal Environment, In: *Biogeochemistry of Marine Dissolved Organic Matter*, A. H. Dennis and A. C. Craig (Eds.), pp. 509–546, Academic Press, San Diego.

Boss, E., W. S. Pegau, J. R. V. Zaneveld, and A. H. Barnard (2001), Spatial and temporal variability of absorption by dissolved matter at a continental shelf, *J. Geophys. Res.*, *106*, 9499–9507.

Bowers, D. G., and H. L. Brett (2008), The relationship between CDOM and salinity in estuaries: An analytical and graphical solution, *J. Mar. Systems*, *73*, 1–7.

Carder, K. L., F. R. Chen, Z. Lee, S. K. Hawes, and J. P. Cannizzaro (2003), MODIS ocean science team algorithm theoretical basis document, *ATBD 19*, pp. 67, NASA, Washington, DC. (Available at http://modis.gsfc. nasa.gov/data/atbd/atbd_mod19.pdf)

Chen, C. T. A. (2008), Distributions of nutrients in the East China Sea and the South China Sea connection, *J. Oceanogr.*, *64*, 737–751.

Chen, C. T. A. (2009), Chemical and physical fronts in the Bohai, Yellow and East China seas, *J. Mar. Systems*, *78*, 394–410.

Chen, C. T. A., W. D. Zhai, and M. H. Dai (2008), Riverine input and air-sea CO_2 exchanges near the Changjiang (Yangtze River) Estuary: Status quo and implication on possible future changes in metabolic status, *Cont. Shelf Res.*, *28*, 1476–1482.

Chen, C.-C., F.-K. Shiah, K.-P. Chiang, G.-C. Gong, and W. M. Kemp (2009), Effects of the Changjiang (Yangtze) River discharge on planktonic community respiration in the East China Sea, *J. Geophys. Res.*, *114*, C03005, doi: 10.1029/2008JC004891.

Chen, R. F., and G. B. Gardner (2004), High-resolution measurements of chromophoric dissolved organic matter in the Mississippi and Atchafalaya River plume regions, *Mar. Chem.*, *89*(1-4), 103–125.

Chen, X., L Zhu, and H. Zhang (2007a), Numerical simulation of summer circulation in the East China Sea and its application in estimating the sources of red tides in the Yangtze River Estuary and adjacent sea areas, *J. Hydro., Ser. B*, *19*(3), 272–281.

Chen, Z. Q., Y. Li, and J. M. Pan (2004), Distributions of colored dissolved organic matter and dissolved organic carbon in the Pearl River Estuary, China, *Cont. Shelf Res.*, *24*(16), 1845–1856.

Chen, Z., C. Hu, R. N. Conmy, F. Muller-Karger, and P. Swarzenski (2007b), Colored dissolved organic matter in Tampa Bay, Florida, *Mar. Chem.*, *104*, 98–109.

Del Castillo, C. E., and R. L. Miller (2008), On the use of ocean color remote sensing to measure the transport of dissolved organic carbon by the Mississippi River plume, *Remote Sens. Environ.*, *112*, 836–844.

Del Vecchio, R., and A. Subramaniam (2004), Influence of the Amazon River on the surface optical properties of the western tropical North Atlantic Ocean, *J. Geophys. Res.*, *109*, C11001, doi: 10.1029/2004JC002503.

Doxaran, D., J. M. Froidefond, S. Lavender, and P. Castaing (2002), Spectral signature of highly turbid water application with SPOT data to quantify suspended particulate matter concentration, *Remote Sens. Environ.*, *81*(2), 149–161.

Fang, G., B. Zhao, and Y. Zhu (1991), Water volume transport through the Taiwan Strait and the continental shelf of the East China Sea measured with current meters. In: *Oceanography of Asian Marginal Seas*, K. Takano (Ed.), pp. 345–358, Elsevier, New York.

Fichot, C. G., and R. Benner (2011), A novel method to estimate DOC concentrations from CDOM absorption coefficients in coastal waters, *Geophys. Res. Lett.*, *38*, L03610, doi: 10.1029/2010GL046152.

Font, J., A. Camps, A. Borges, M. Martín-Neira, J. Boutin, N. Reul, Y. H. Kerr, A. Hahne, and S. Mecklenburg (2010), SMOS: The challenging sea surface salinity measurement from space, *Proc. IEEE*, *98*(5), 649–665, doi: 10.1109/JPROC.2009.2033096.

Gong, G.-C. (2004), Absorption coefficients of colored dissolved organic matter in the surface waters of the East China Sea, *Terr. Atmos. Oceanic Sci.*, *15*, 75–87.

Gong, G.-C., K.-K. Liu, K.-P. Chiang, T.-M. Hsiung, J. Chang, C.-C. Chen, C.-C. Hung, W.-C. Chou, C.-C. Chung, H.-Y. Chen, F.-K. Shiah, A.-Y. Tsai, C.-H. Hsieh, J.-C. Shiao, C.-M. Tseng, S.-C. Hsu, H.-J. Lee, M.-A. Lee, I.-I. Lin, and F. Tsai (2011), Yangtze River floods enhance coastal ocean phytoplankton biomass and potential fish production, *Geophys. Res. Lett.*, *38*, L13603, doi: 10.1029/2011GL047519.

Guo, W.-D., C. A. Stedmon, Y.-C. Han, F. Wu, X.-X. Yu, and M.-H. Hu (2007), The conservative and non-conservative behavior of chromophoric dissolved organic mater in Chinese estuarine waters, *Mar. Chem.*, *107*, 357–366.

He, X. Q., D. L. Pan, and Z. H. Mao (2004), Atmospheric correction of SeaWiFS imagery for turbid coastal and inland waters, *Acta Oceanol. Sini.*, *23*(4), 609–615.

He, X. Q., Y. Bai, D. L. Pan, J. W. Tang, and D. F. Wang (2012), Atmospheric correction of satellite ocean color imagery using the ultraviolet wavelength for highly turbid waters, *Opt. Express*, *20*(18): 20754–20770.

Helms, J. R., A. Stubbins, J. D. Ritchie, E. C. Minor, D. J. Kieber, and K. Mopper (2008), Absorption spectral slopes and slope ratios as indicators of molecular weight, source, and photobleaching of chromophoric dissolved organic matter, *Limnol. Oceanogr.*, *53*(3), 955–969.

Hernes, P. J., and R. Benner (2003), Photochemical and microbial degradation of dissolved lignin phenols: Implications for the fate of terrigenous dissolved organic matter in marine environments, *J. Geophys. Res.*, *108*(C9), 3291, doi:10.1029/2002JC001421.

Hitchcock, G. L., R. F. Chen, G. B. Gardner, and W. J. Wiseman Jr. (2004), A Lagrangian view of fluorescent chromophoric dissolved organic matter distributions in the Mississippi River plume, *Mar. Chem.*, *89*, 225–239.

Hong, H. S., J. Y. Wu, S. L. Shang, and C. M. Hu (2005), Absorption and fluorescence of chromophoric dissolved organic matter in the Pearl River Estuary, South China, *Mar. Chem.*, *97*, 78–89.

Hu, C. M., E. T. Montgomery, R. W. Schmitt, and F. E. Muller-Karger (2004), The dispersal of the Amazon and Orinoco river water in the tropical Atlantic and Caribbean Sea: Observations from space and S-PALACE floats, *Deep Sea Res., Part II*, *51*, 1151–1171.

Hu, C. M., Z. Li, E. Muller-Karger, L. Carder, and J. J. Walsh (2006). Ocean color reveals phase shift between marine plants and yellow substance, *Geoscience and Remote Sensing Letters, IEEE*, *3*(2), 262–266.

Isobe, A., and T. Matsuno (2008), Long-distance nutrient-transport process in the Changjiang River plume on the East China Sea shelf in summer, *J. Geophys. Res.*, *113*, C04006, doi:10.1029/2007JC004248.

Johnson, D. R., J. Miller, and O. Schofield (2003), Dynamics and optics of the Hudson River outflow plume, *J. Geophys. Res.*, *108*(C10), 3323, doi: 10.1029/2002JC001485.

Kerr, Y. H., P. Waldteufel, J. Wigneron, S. Delwart, F. Cabot, J. Boutin, M. J. Escorihuela, J. Font, N. Reul, and C. Gruhier (2010), The SMOS mission: New tool for monitoring key elements of the global water cycle, *Proc. IEEE*, *98*(5), 666–687, doi:10.1109/JPROC.2010.2043032.

Koblinsky, C. J., P. Hildebrand, D. LeVine, F. Pellerano, Y. Chao, W. Wilson, S. Yueh, and G. Lagerloef (2003), Sea surface salinity from space: Science goals and measurement approach, *Radio Sci.*, *38*(4), 8064, doi:10.1029/2001RS002584.

Lagerloef, G. S. E., F. Colomb, D.M. Le Vine, F. Wentz, S. Yueh, C. Ruf, J. Lilly, J. Gunn, Y. Chao, A. de Charon, G. Feldman, and C. Swift (2008), The Aquarius/SAC-D mission: designed to meet the salinity remote-sensing challenge, *Oceanography*, *20*, 68–81.

Lee, Z., K. L. Carder, R. G. Steward, T. G. Peacock, C. O. Davis, and J. L. Mueller (1996), *Protocols for measurement of remote-sensing reflectance from clear to turbid waters*, Presented at SeaWiFS Workshop, Halifax.

Lee, Z. P. (Ed.) (2006), Remote sensing of inherent optical properties: Fundamentals, tests of algorithms, and applications, *Reports of the International Ocean-Colour Coordinating Group, No. 5*, IOCCG, Dartmouth, Canada.

Lee, Z. P., K. L. Carder, and R. A. Arnone (2002), Deriving inherent optical properties from water color: A multi-band quasi-analytical algorithm for optically deep waters, *Appl. Opt.*, *41*(27), 5755–5772, doi:10.1364/AO.41.005755.

Liu, Z. L., and J. P. Gan (2012), Variability of the Kuroshio in the East China Sea derived from satellite altimetry data, *Deep Sea Res., Part I*, *59*, 25–36.

Miller, R. L., M. Belz, C. D. Castillo, and R. Trzaska (2002), Determining CDOM absorption spectra in diverse coastal environments using a multiple pathlength, liquid core waveguide system, *Cont. Shelf Res.*, *22*, 1301–1310.

Mitchell, B.G., M. Kahru, J. Wieland and M. Stramska (2000), Determination of spectral absorption coefficients of particles, dissolved material and phytoplankton for discrete water samples, In: *Ocean optics protocols for satellite ocean color sensor validation*, edited by G. S. Fargion and J. L. Mueller, Rev. 2, pp. 125–153, Goddard Space Flight Space Center, Greenbelt, Md.

Molleri, G. S. F., E. M.L. de M. Novo, and M. Kampel (2010), Space-time variability of the Amazon River plume based on satellite ocean color, *Cont. Shelf Res.*, *30*, 342–352.

Moon, J. H., I. C. Pang and J. H. Yong (2009), Response of the Changjiang Diluted Water around Jeju Island to external forcings: A modeling study of 2002 and 2006. *Cont. Shelf Res.*, *29*, 1549–1564.

Morel, A. and B. Gentilli (1991), Diffuse reflectance of oceanic waters: Its dependence on sun angle as influenced by the molecular scattering contribution, *Appl. Opt.*, *30*(30), 4427–4438.

Mueller, J. L., G. S. Fargion, and C. R. McClain (Eds.) (2003), Biogeochemical and bio-optical measurements and data analysis methods, *NASA Tech.*

Memo., NASA TM-2003-211621, Rev. 4, vol. 2, Goddard Space Flight Space Center, Maryland.

Murphy, K. R., C. Stedmon, T.D. Waite, and G.M. Ruiz(2008), Distinguishing between terrestrial and autochthonous organic matter sources in marine environments using fluorescence spectroscopy, *Mar. Chem.*, *108*, 40–58.

Nelson N, D. Siegel, and A. Michaels (1998), Seasonal dynamics of colored dissolved material in the Sargasso Sea, *Deep Sea Res., Part I*, *45*(6), 931–957.

Nelson, N. B., D. A. Siegel, C. A. Carlson, and C. M. Swan (2010), Tracing global biogeochemical cycles and meridional overturning circulation using chromophoric dissolved organic matter, *Geophys. Res. Lett.*, *37*, L03610, doi:10.1029/2009GL042325.

Palacios, S. L., T. D. Peterson, and R. M. Kudela (2009), Development of synthetic salinity from remote sensing for the Columbia River plume, *J. Geophys. Res.*, *114*, C00B05, doi:10.1029/2008JC004895.

Prieur, L., and S. Sathyendranath (1981), An optical classification of coastal and oceanic waters based on the specific absorption of phytoplankton pigments, dissolved organic matter, and other particulate materials, *Limnol. Oceanogr.*, *26*, 671–689.

Reul, N., S. Saux-Picart, B. Chapron, D. Vandemark, J. Tournadre, and J. Salisbury (2009), Demonstration of ocean surface salinity microwave measurements from space using AMSR-E data over the Amazon plume, *Geophys. Res. Lett.*, *36*, L13607, doi:10.1029/2009GL038860.

Ryu, J. H., J. K. Choi, J. Eom, and J. H. Ahn (2011), Temporal variation in Korean coastal waters using Geostationary Ocean Color Imager, *J. Coast. Res.*, *SI64*, 1731–1735.

Salisbury, J., D. Vandemark, J. Campbell, C. Hunt, D. Wisser, N. Reul, and B. Chapron (2011), Spatial and temporal coherence between Amazon River discharge, salinity, and light absorption by colored organic carbon in western tropical Atlantic surface waters, *J. Geophys. Res.*, *116*, C00H02, doi:10.1029/2011JC006989.

Sasaki, H., E. Siswanto, K. Nishiuchi, K. Tanaka, T. Hasegawa, and J. Ishizaka (2008), Mapping the low salinity Changjiang Diluted Water using satellite-retrieved colored dissolved organic matter (CDOM) in the East China Sea during high river flow season, *Geophys. Res. Lett.*, *35*, L04604, doi: 10.1029/2007GL032637.

Sathyendranath, S. (Ed.) (2000), Remote sensing of ocean colour in coastal, and other optically-complex, waters., *Reports of the International Ocean-Colour Coordinating Group, No. 3*, IOCCG, Dartmouth, Canada.

Siddorn, J. R., D. G. Bowers, and A. M. Hoguane (2001), Detecting the Zambezi River plume using observed optical properties, *Mar. Pollut. Bull.*, *42*, 942–950.

Siegel, D. A., S. Maritorena, N. B. Nelson, D. A. Hansell, and M. Lorenzi-Kayser (2002), Global distribution and dynamics of colored dissolved and detrital organic materials, *J. Geophys. Res.*, *107*(C12), 3228, doi:10.1029/2001JC000965.

Stedmon, C. A., C. L. Osburn, and T. Kragh(2010), Tracing water mass mixing in the Baltic-North Sea transition zone using the optical properties of coloured dissolved organic matter, *Estuarine, Coastal and Shelf Science*, *87*,156–162.

Stedmon, C.A., and S. Markager (2001), The optics of chromophoric dissolved organic matter (CDOM) in the Greenland Sea: An algorithm for differentiation between marine and terrestrially derived organic matter, *Limnol. Oceanogr.*, *46*, 2087–2093.

Stedmon, C.A., and S. Markager (2005), Tracing the production and degradation of autochthonous fractions of dissolved organic matter using fluorescence analysis, *Limnol. Oceanogr.*, *50*, 1415–1426.

Su, J. and K. Wang, (1989), Changjiang River plume and suspended sediment transport in Hangzhou Bay, *Cont. Shelf Res.*, *9*(1), 93–111.

Tsunogai, S., S. Watanabe, and T. Sato (1999), Is there a continental shelf pump for the absorption of atmospheric CO_2?, *Tellus, Ser. B*, *51*, 701–712, doi:10.1034/j.1600-0889.1999.t01-2-00010.x.

Twardowski, M. J., and P. L. Donaghay (2001), Separating in situ and terrigenous sources of absorption by dissolved materials in coastal waters, *J. Geophys. Res.*, *106*(C2), 2545–2560.

Twardowski, M.S., E. Boss, J. M. Sullivan, and L. Percy (2004), Modeling the spectral shape of absorption by chromophoric dissolved organic matter, *Mar. Chem.*, *89*, 69–88.

Vodacek, A., N. V. Blough, M. D. Degrandpre, E. T. Peltzer, and R. K. Nelson (1997), Seasonal variation of CDOM and DOC in the Middle Atlantic Bight: Terrestrial inputs and photo-oxidation, *Limnol. Oceanogr.*, *42*, 674–686.

Wang, M., J. Tang, and W. Shi (2007), MODIS-derived ocean color products along the China east coastal region, *Geophys. Res. Lett.*, *34*, L06611, doi:10.1029/2006GL028599.

Werdell, P. J., and S. W. Bailey (2005), An improved in situ bio-optical data set for ocean color algorithm development and satellite data product validation, *Remote Sens. Environ.*, *98*(1), 122–140.

Xie, D., Z. Wang, S. Gao, and H. J. De Vriend (2009), Modeling the tidal channel morphodynamics in a macro-tidal embayment, Hangzhou Bay, China, *Cont. Shelf Res.*, *29*, 1757–1767.

Yuan, D. and Y. Hsueh (2010), Dynamics of the cross-shelf circulation in the Yellow and East China Seas in winter, *Deep Sea Res., Part II*, *57*, 1745–1761.

Yuan, D., J. Zhu, C. Li, and D. Hu (2008), A cross-shelf circulation in the Yellow and East China Seas indicated by MODIS satellite observations, *J. Mar. Systems*, *70*, 134–149.

Zhang, J., Y. Wu, T. C. Jennerjahn, V. Ittekkot, and Q. He (2007), Distribution of organic matter in the Changjiang (Yangtze River) Estuary and their stable carbon and nitrogen isotopic ratios: Implications for source discrimination and sedimentary dynamics, *Mar. Chem.*, *106*, 111–126.

Zhao, J., W. X. Cao, G. F. Wang, D. T. Yang, Y. Z. Yang, Z. H. Sun, W. Z. Zhou, and S. J. Liang (2009), The variations in optical properties of CDOM throughout an algal bloom event, *Estuarine Coastal Shelf Sci.*, *82*, 225–232.

Zhou, M., T. Yan, and J. Zou (2003), Preliminary analysis of the characteristics of red tide areas in Changjiang River Estuary and its adjacent sea, *Chin. J. Appl. Ecol.*, *14*(7), 1031–1038(in Chinese).

Zhu, W., Q. Yu, Y. Q. Tian, R. F. Chen, and G. B. Gardner (2011), Estimation of chromophoric dissolved organic matter in the Mississippi and Atchafalaya river plume regions using above-surface hyperspectral remote sensing, *J. Geophys. Res.*, *116*, C02011, doi:10.1029/2010JC006523.